Bioactive Materials 11 (2022) 283–299

Contents lists available at ScienceDirect

Bioactive Materials

journal homepage: www.keaipublishing.com/en/journals/bioactive-materials

Pharmacological manipulation of macrophage autophagy effectively rejuvenates the regenerative potential of biodegrading vascular graft in aging body

Wanli Chen [a,b,1], Weiwei Xiao [a,1], Xuzheng Liu [a], Pingping Yuan [a], Siqian Zhang [a], Yinggang Wang [a], Wei Wu [a,*]

[a] State Key Laboratory of Military Stomatology & National Clinical Research Center for Oral Diseases & Shaanxi Key Laboratory of Stomatology, Department of Oral & Maxillofacial Surgery, School of Stomatology, The Fourth Military Medical University, Xi'an, Shaanxi, China
[b] School & Hospital of Stomatology, Tongji University, Shanghai Engineering Research Center of Tooth Restoration and Regeneration, 399 Middle Yanchang Road, Shanghai 200072, China

ARTICLE INFO

Keywords:
Autophagy
Macrophages
Inflammation
Aging
Fast-degradation materials

ABSTRACT

Declined regenerative potential and aggravated inflammation upon aging create an inappropriate environment for arterial regeneration. Macrophages are one of vital effector cells in the immune microenvironment, especially during biomaterials mediated repairing process. Here, we revealed that the macrophage autophagy decreased with aging, which led to aggravated inflammation, thereby causing poor vascular remodeling of artificial grafts in aging body. Through loading the autophagy-targeted drugs, rapamycin and 3-MA (3-methyladenine), in PCL (polycaprolactone) sheath of the PGS (poly glycerol sebacate) - PCL vascular graft, the essential role of macrophage autophagy was confirmed in regulating macrophage polarization and biomaterial degradation. Moreover, the utilization of rapamycin promoted anti-inflammatory polarization of macrophage by activating autophagy, which further promoted myogenic differentiation of vascular progenitor cells and accelerated endothelialization. Our study elucidated the contribution of pharmacological manipulation of macrophage autophagy in promoting regeneration of small caliber artery, which may pave a new avenue for clinical translation of vascular grafts in aging body.

1. Introduction

In vivo performance of vascular graft is profoundly influenced by material properties, circulating blood and perivascular environment, which are orchestrated locally via distinct cellular interactions within the vascular microenvironment [1]. Perivascular adipose tissue (PVAT), one indispensable component of this microenvironment, situates outside the adventitial layer and surrounds the majority of systemic blood vessels [2]. Vascular biology researches have revealed that abundant vascular precursor cells (VPCs) and immune cells reside in the adventitial layer and PVAT [3]. A series of growth factors and cytokines secreted by pro-inflammatory and anti-inflammatory cells regulate the differentiation of VPCs [4]. For example, PDGF-BB secreted by anti-inflammatory macrophages can promote the myogenic differentiation of vascular progenitor cells. The crosstalk between macrophages and stem cells plays key role in myogenesis of vascular graft [5]. The general strategy promoting vascular regeneration involves targeting vascular precursor cells, enhancing endothelialization, and fabricating bioactive biomaterials [6]. However, chronic inflammation caused by most vascular biomaterials greatly restricts the effect of vascular regeneration. Given the importance of an inflammation-mediated process in transformation from vascular grafts into neoartery [7], endowing vascular grafts with immunomodulatory property offers new approach to promoting vascular regeneration.

Peer review under responsibility of KeAi Communications Co., Ltd.

* Corresponding author. State Key Laboratory of Military Stomatology & National Clinical Research Center for Oral Diseases & Shaanxi Key Laboratory of Stomatology, Department of Oral & Maxillofacial Surgery, School of Stomatology, the Fourth Military Medical University, Changle West Road 145, Xi'an, Shaanxi, 710032, China.
E-mail address: wuweidds@126.com (W. Wu).
[1] These authors contributed to the work equally and should be regarded as co-first authors.

https://doi.org/10.1016/j.bioactmat.2021.09.027
Received 18 May 2021; Received in revised form 28 August 2021; Accepted 22 September 2021
Available online 20 October 2021

Poly glycerol sebacate-polycaprolactone (PGS-PCL) vascular graft is a cell-free synthetic graft, which can transform into a vessel-like structure in situ by exploiting the host's inherent regenerating capacity [8]. Despite successful regeneration of small caliber artery in young rats, vascular remodeling of PGS-PCL graft is compromised and even failed when it is implanted into the aging body [9,10]. Grafts' occlusion, rupture, dilation or aneurysm presented in aging body impeded the progression of translational study. It has been revealed that inflammation accompanied with aging greatly influenced tissue repair [11,12]. For PGS-PCL composite grafts, both acute inflammations initiated by fast degrading PGS and chronic inflammations caused by slow degrading PCL cannot be resolved by senescent homeostatic mechanisms and may even worsen with aging, which eventually results in adverse vascular remodeling [5]. The rational design of biodegradable vascular grafts in aging body remains to be investigated.

Our previous study revealed an interesting phenomenon that autophagy of the recruited macrophages in graft was significantly activated by the immunoregulatory peptides [5]. Autophagy is fundamental to eukaryotic cell homeostasis [13] and is a critical cyto-adaptive response to environmental stresses including starvation, ischemia, hypoxia and infection [14,15]. For the pioneering macrophages, autophagy protects them against stress of ischemia and hypoxia in grafts. It has been demonstrated that the decreased autophagy in aged macrophages leads to functional decline and aberrant inflammatory cytokine production, which stressed significance of autophagy in the regulation of inflammation associated with aging [16]. Autophagic dysregulation may be a common pathway through which vascular aging and associated pathologies develop [17], and administrating autophagy activators appears to reverse the arterial aging [18].

Macrophages, playing significant roles in innate and adaptive immunity, may typically polarize into the pro-inflammatory M1 and the anti-inflammatory M2 phenotypes [19,20]. Recent evidences suggest that autophagy can regulate macrophage M1/M2 polarization under different inflammatory conditions [21]. It is reported that selective autophagy induced NF-κB lysosomal degradation in hepatoma-derived M2 macrophage differentiation [22]. However, the specific mechanism by which autophagy regulates macrophage polarization has not been fully elucidated. Emerging evidence reveals that the targeting rapamycin (mTOR) pathway plays key roles in macrophage polarization in mammalian [23–25]. mTOR is a major regulator of autophagy, inhibiting mTOR may increase autophagy levels [26]. Inhibitory use of rapamycin to mTORC1 or specific knockout of mTORC1 in macrophages can polarize macrophages to M2, which may inhibit synovial inflammation and delay the progression of osteoarthritis in mice [27,28]. Given the crucial roles of macrophages and autophagy in vascular aging, as well as their correlation in biological activities, the aims of this work were to clarify the role of autophagy in macrophage polarization and their implications for vascular remodeling in aging bodies.

For regulating macrophage autophagy, two basic requirements need to be satisfied: the microstructure of vascular grafts should be opening for recruitment of the macrophages; adequately physicochemical stability should be acquired for drug loading and releasing. Currently, most arterial substitutes are bioinert materials and exhibit limited host cell infiltration [29,30]. Different from the slow-degrading bioinert materials, the fast-degrading porous PGS scaffold was favorable for rapid and extensive infiltration of macrophages [10]. However, drug loading remains a technical challenge for fast degrading elastic vascular grafts. Conventionally, the fabrication of PGS porous elastomer contains two critical processes: salt leaching ensures the sufficient removal of procoagulant NaCl particles in the PGS core and heparin coating improves thromboresistance [8]. Unfortunately, both of them may flow away the loaded drugs before implantation. Here, we replaced NaCl with sodium citrate which is a well-recognized anticoagulant, and can resistant luminal clotting and maintain catheter patency [31]. The use of sodium citrate avoids the drug-loss caused by salt leaching and heparin coating. Base on the PGS-sodium citrate core, immunomodulatory vascular grafts were fabricated through incorporating autophagy-targeted drugs (rapamycin and 3-MA) into PCL sheath of vascular grafts, and macrophage infiltration and autophagic alternation were analyzed. The further regenerative potential of artery in aging rats were evaluated at the state of autophagy inhibition and autophagy activation, in an effort to identify the ideal candidate design for vascular grafts in aging body.

2. Materials and methods

2.1. Fabrication of the drug loaded vascular grafts

The vascular grafts were composed of PGS core and PCL/collagen nanofibrous sheath as described previously [5]. In brief, the sodium citrate tubes and the NaCl tubes were instilled with PGS respectively and crosslinked at 150 °C for 24 h to obtain two different PGS cores. PCL (Mn 80 kDa; Aldrich, MO, USA) was dissolved in 2,2,2-trifluoroethanol at 14% weight/volume (w/v). Collagen (Collagen type I from bovine Achilles tendon, Sigma) was dissolved in 1,1,1,3,3,3-hexafluoroisopropanol (HFIP) at 8% w/v. The rapamycin, 3-methyladenine (3-MA) and trehalose were dissolved in de-ionized water with the same concentration (1 mg/ml). Then, rapamycin, 3-MA and trehalose solution were mixed with collagen solutions at 4:1 (v/v) to acquire drug-mixed collagen solution respectively. PBS was also mixed with collagen solutions at 4:1 (v/v) as the control. The PCL solution (2.5 ml/h) and drug-mixed collagen solution (1 ml/h) were co-electrospun onto the rotating PGS core template at 120 rpm for 3 min. After that, the PGS-NaCl cores with PCL-Col sheath were soaked in de-ionized water for 24h to ensure the completely removal of NaCl. Meanwhile, the PGS-Sodium citrate cores with PCL-Col sheath were nebulized for 1 min to obtain the elastomeric vascular grafts that were easy to suture. Finally, these two kinds of composite grafts were sterilized by ultraviolet radiation for 60 min and stored at −80 °C until use.

2.2. Characterization of the drug loaded vascular grafts

Two different drug loaded vascular grafts (PGS-Sodium citrate core and PGS-NaCl core) were characterized for structure and releasing patterns of loaded drugs. The cross-sections and outer surface of sheath were examined by Scanning Electronic Microscopy (SEM, Hitachi, s-4800, Japan), and sheath thickness was measured as previously described [10]. In addition, the nanostructure of these sheaths was investigated by Atomic Force Microscope (AFM, Dimension Icon, Bruker, USA). Next, we test the drug releasing patterns of these two vascular grafts in vitro. Briefly, drug loaded vascular grafts (1 cm) were incubated in RPMI-1640 (1 ml; containing 1% BSA) at 37 °C. At various time points, 0.5 ml supernatant were removed from the chambers and analyzed via high performance liquid chromatography (HPLC). The initial drug Loading contents of these two vascular grafts (1 cm) were calculated with the following equations:

$$W_{Col} = W_{3min\text{-}PCL/Col} - W_{3min\text{-}PCL}$$

$$W_{drug} = [(V_{drug} \times C_{drug})/(V_{Col} \times C_{Col}) \times W_{Col}$$

The $W_{3min\text{-}PCL/Col}$ is the weight of 3min-PCL/Col graft. The $W_{3min\text{-}PCL}$ is the weight of 3min-PCL graft. Both of them were measured by an electronic scale. The W_{drug} is the weight of loaded drugs on 3min-PCL/Col graft. The W_{Col} is the weight of spraying collagen on 3min-PCL/Col graft. V_{drug} means the volume of the drug (rapamycin or 3-MA) solution, and V_{Col} means the volume of the collagen solution. V_{drug}: V_{Col} = 1:4 as previously mentioned. C_{drug} means the concentration of the drug solution and C_{drug} = 1 mg/ml as previously mentioned. C_{Col} means the concentration of the collagen solution and C_{Col} = 80 mg/ml.

2.3. Animal grouping and surgery

All procedures were approved by the Animal Experiments Ethical

Committee of Fourth Military Medical University and complied with the Guide for Care and Use of Laboratory Animals. Male Sprague Dawley (SD) rats (Young: 10–12 weeks, weight = 350–400 g, n = 25; Aging: 18–25 months, weight = 550–600 g, n = 59) were purchased from the fourth military medical university laboratory animal center (Xi'an). To compare the effects of aging on vascular remodeling, 15 young and 15 aging rats were used for PGS-PCL vascular graft implantation respectively. 7 rats from each group were harvested 2 weeks postoperatively and another 8 after 6 months. Two weeks after implantation, three independent patent sample in each group were harvested for immunofluorescence staining (vWF, CD68, CD206, and iNOS), western blotting (LC3), and transmission electron microscopy (TEM). Six months after implantation, three independent patent samples in each group were harvested for immunofluorescence staining (Elastin, Collagen I, and Collagen III), elastin and collagen quantification, and histological staining (hematoxylin and eosin (H&E), Verhoeffe-Van Gieson (VVG), Masson's trichrome (MTS), and Alizarin red staining (ARS)).

To test the crucial role of macrophages, GFP+ (green fluorescent protein positive) macrophages were transplanted on the grafts after macrophage depletion. Clodronate liposomes (5 mg/ml, Netherlands) were used to deplete the monocytes/macrophages in PVAT as reported previously [5]. GFP + macrophages were derived from bone marrow which isolated from the GFP-transgenic SD rats (Cyagen Biosciences Inc., China). Matrigels containing GFP + macrophages were applied surrounding the adventitia of rapamycin loaded grafts (n = 5). Totally 20 aging rats were assigned randomly into 4 groups. Group 1 (PBS): Rapamycin loaded grafts were implanted with PBS liposomes injection. Group 2 (Control): Rapamycin loaded grafts were implanted with clodronate liposomes injection. Group 3 (GFP + Rapa): Rapamycin loaded grafts were implanted with GFP + macrophages transplantation after clodronate liposomes injection. Group 4 (GFP + PBS): Rapamycin loaded grafts were implanted with GFP + macrophages transplantation after PBS liposomes injection.

To evaluate the drug-loaded grafts in long term (6 months), totally 24 aging rats were assigned randomly into PBS, rapamycin and 3-MA groups, 8 rats in each group. Besides, to evaluate the drug-loaded grafts in short term (2 weeks), totally 18 aging rats were assigned randomly into PBS, rapamycin, 3-MA and trehalose groups, 5 rats in PBS, Rapa and 3-MA group and 3 rats in trehalose group. we performed interpositional implantation in rat abdominal aortas as described before [8]. In brief, rats were anesthetized by isoflurane inhalation (5% for induction, then 2% for maintenance). A midline laparotomy incision was performed before the abdominal aorta was isolated, clamped, and transected. The vascular grafts (1.0 mm in inner diameter and 1.0 cm in length) were sewed in an end-to-end fashion with 10 interrupted stitches using 9-0 monofilament nylon sutures. No anticoagulation or antiplatelet treatment was administrated postoperatively. All of the animals were sacrificed by injection of overdose pentobarbital sodium (Sigma, USA) at predetermined time-points (2 weeks and 6 months) after the neoarteries were harvested for further experiments.

2.4. Histological analysis of the explanted vascular grafts

OCT-embedded (Sakura Finetek, CA, USA) explants were frozen rapidly with liquid nitrogen and then cross sectioned into 6 μm thick pieces. After fixing with 4% paraformaldehyde for 5 min, the sections were stained with hematoxylin and eosin (H&E), Verhoeffe-Van Gieson (VVG), and Masson's trichrome (MTS). All histological images were observed with an upright fluorescence microscope (DM6000B, Leica, Germany) in brightfield or under polarized light. Polarized H&E images from three different samples (n = 3) in each group at the designated time points were used to quantify area of polymer residuals. The PCL residuals visualized with polarized light presented as specific white birefringence, while no birefringence on PGS. The PGS residuals visualized with brightfield presented as slightly stained porous structure. The areas of polymer residuals were measured using Image J software (NIH). Percentage of polymer residuals were calculated by following formulas:

$$P_{PGS}=S_1/S_2 \times 100\%$$

$$P_{PCL}=S_3/S_4 \times 100\%$$

P_{PGS} means the percentage of PGS residuals, $S_1$is the area of PGS residuals in H&E images, S_2 is the area of PGS in the PGS-PCL grafts before implantation. P_{PCL} means the percentage of PCL residuals. S_3 is the area of PCL residuals in polarized light images, and S_4 is the area of PCL sheath of original PGS-PCL grafts in polarized light image.

2.5. TEM imaging

Samples prepared for TEM were first cut into 2 mm^3 pieces and then fixed overnight at 4 °C in PBS containing 2.5% glutaraldehyde. After fixation in 1% OsO_4 solution for 1 h at room temperature, these samples were dehydrated with gradient ethanol solutions and embedded in epoxy resin. Ultrathin sections (70–90 nm) were prepared with an ultramicrotome (Leica Microanalysis) and stained with uranyl acetate/lead citrate. The prepared sections were imaged under a transmission electron microscope (JEM1400PLUS, Japan).

2.6. Immunofluorescence staining

Immunofluorescence staining was performed as previously described [5]. Smooth muscle cells were stained using mouse anti-SM-MHC (Abcam, UK) primary antibodies. Endothelial cell staining was performed using rabbit anti-vWF (Abcam, USA) primary antibody. The vascular precursor cell was stained using rabbit anti-Sca-1 (Millipore, Germany). For elastin and collagen staining, slides were incubated with rabbit anti-Elastin (Abcam, UK), mouse anti-Collagen I (Abcam, UK) and mouse anti-Collagen III (Abcam, UK). To observe inflammatory cells in the explanted grafts, mouse anti-CD68 (Abcam, UK), rabbit anti-iNOS (Abcam, UK) and rabbit anti-CD206 (Abcam, UK) were used as primary antibodies. After overnight incubated at 4 °C, slides were washed twice with PBS solution and incubated with the respective fluorescein isothiocyanate-conjugated secondary antibodies for 60 min at 37 °C. The samples were observed using an Olympus Flu view 1000 confocal microscope (Japan). Tissue slides pretreated without a primary antibody were used as negative controls. Cell populations were determined based on cell counts from each image on six different parts (12, 2, 4, 6, 8, and 10 o'clock positions). Data were collected from three different samples in each group. Details of the primary antibodies are listed in Table S1.

2.7. Cell culture

Bone marrow derived monocytes were obtained from the freshly isolated bone marrow of the femur and tibia of 2 weeks old SD rats. The monocytes were isolated using the differential adhesion method as previously reported [32,33]. Macrophages were differentiated from bone marrow derived monocytes in the presence of macrophage colony stimulating factor (M-CSF, Peprotech) and then seeded on the PBS, Rapa, and 3-MA loaded scaffolds. The circular scaffold was composed of two parts, the lower PGS scaffold and upper PCL sheath. All of them were 2 mm thick and 15 mm in diameter. After 7 days of culture, cells adhered on the scaffolds were harvested for further analysis.

To investigate the crosstalk between macrophages seeded on drug-loaded scaffolds and PVAT-derived Sca-1+ cells, rat PVAT-derived Sca-1+ cells were cocultured with macrophages via the transwell system (pore size, 0.4 μm; Thermo Scientific). After coculturing for 7 days, Sca-1+ cells in the upper chamber were collected for further analysis. Each experiment was repeated in triplicate at least three times.

2.8. Flow cytometry

In order to simulate a drug released scaffold microenvironment,

macrophages were seeded (1×10^6) on PBS, Rapamycin and 3-methyladenine loaded PGS-PCL constructs respectively. After 36 h' incubation, the macrophages were collected following detachment using 0.25% trypsin and rinsing with PBS, and apoptosis of cells in three groups were analyzed through flowcytometry. In brief, macrophages were resuspended in 500 μl binding buffer, then were treated with 5 μl Annexin V-FITC and 5 μl PI. After 15-min reaction at 25 °C, the mixture was analyzed using a BD FACS Calibur™ flow cytometer and BD FACS Diva™ 6.0 software (BD Biosciences).

To isolate the macrophages from the tissue in young and aging groups, the sample of the tissue (2 × 5 mm) were minced in precooled PBS and digested with Type I collagenase (2 mg/ml, Gibco, USA) for 30min at 37 °C to obtain single-cell suspension [34]. It was then incubated with FITC-conjugated anti-CD68 (Abcam, USA) for 30 min. After washing and resuspending with PBS, the immune-stained cells were isolated by flow cytometry sorting and the purity of sorted cells was examined by flow cytometry (BD Biosciences).

2.9. Western blotting

Total proteins in cell lysates and whole-tissue lysates were harvested using a lysis solution, separated by 10% SDS-PAGE gels, and then transferred to polyvinylidene difluoride membranes and blocked in 5% nonfat milk. Subsequently, ATG5, LC3, p-mTOR/mTOR and p-AMPK/AMPK antibodies were dropped onto the membranes and incubated overnight at 4 °C. The membranes were then treated with a horseradish peroxidase-conjugated secondary antibody and protein bands were detected via enhanced chemiluminescence. Each experiment was performed three times to achieve comparable results. Relative densities were measured using Image J (version: 1.37v) software (Wayne Rasband). Details of the primary antibodies are listed in Table S1.

2.10. Autophagy flux assay

To confirm the induction or inhibition of macrophage autophagy regulated by loading the autophagy-targeted drugs, macrophages were infected with mRFP (mcherry red fluorescent protein)-GFP-LC3 (Hanbio, China) for 72 h and then seeded on PBS, Rapa and 3-MA-loaded scaffolds respectively. Images were obtained using the laser scanning confocal microscope (Olympus, FV1000, Tokyo, Japan) and analyzed using Image J software.

2.11. Statistical analysis

Statistical analyses were performed using SPSS software, version 18.0 (IBM, Chicago, IL, http://www.ibm.com). Continuous variables were expressed as mean ± standard deviation (SD). Comparison of means between two groups was performed using the student t-test. Differences between multiple groups were determined via one-way analysis of variance (ANOVA) followed by Tukey's post hoc analysis. $p < 0.05$ was considered statistically significant.

3. Results

3.1. Impaired vascular remodeling of PGS-PCL grafts in aging bodies

To evaluate the adverse effects of aging on arterial remodeling, we implanted PGS-PCL grafts into the abdominal aortas of 15 aging rats and 15 young rats, respectively (Fig. S1a). Six months later, the patency rates determined via necropsy is 85.71% (6 patent grafts/7 total grafts) in the young group, and 66.67% (4/6) in the aging group (Table S1). To assess endothelialization in two groups, 7 grafts in each group were harvested at 2 weeks postoperatively. Different from the high endothelial cell (EC) coverage of neoarteries in young group (53.76 ± 9.76%), immunofluorescence analysis showed that vWF staining in neoarteries of aging group was scarce (18.75 ± 6.33%) (Figure S 1b, c). Impaired endothelialization on the luminal surface is associated with poor graft patency. Among patent grafts, severe aneurysmal dilatation occurred in five grafts from aging group, while no aneurysm was detected in those from young group (Fig. S1a, Table S1). Further histological analysis showed distinct muscular remodeling between two groups (Fig. S1 d-k). As revealed by H&E staining, grafts from aging group exhibited variant wall thickness, and more dilated luminal areas as compared with those from the young group (Figs. S1d and e). Elastic fibers, presented as black stained with VVG, were evenly and circumferentially distributed in neoarteries of young group (Fig. S1f). In contrast, few elastic fibers formed in extracellular matrix (ECM) of neoarteries in aging group (Fig. S1f). In accordance with VVG staining, immunofluorescent staining confirmed that substantial elastin was circumferentially aligned in young group, while elastin production was weak in newly formed ECM of neoarteries from aging group (Fig. S1g). Quantitatively, the elastin content was 5.39 ± 1.09 μg/mg in the aging group, which was significantly lower than that of young group (11.28 ± 1.22 μg/mg, $p < 0.05$) (Fig. S1l). Masson's trichrome staining showed overall distribution of collagen fibers in two groups (Fig. S1h). Although no significant difference was detected between the collagen content in these two groups (young vs. aging: 71.56 ± 3.60 μg/mg vs. 68.41 ± 5.30 μg/mg, $p > 0.05$) (Fig. S1m), the main component in neoarteries of the aging group was COL-I, a major ECM component that represented fibrosis (Figs. S1j, k, n). "Alizarin red" staining revealed that calcification, which was not observed in the young group, occurred in vessel walls of aging-group (Figs. S1i and o). These findings suggested impaired production of elastin and aggravated fibrosis upon aging would cause severe aneurysms or arterial calcification in the neoarteries from PGS-PCL vascular grafts.

3.2. Aging-induced reduction of autophagy and increase of pro-inflammatory macrophages polarization

Given that autophagy is closely related to aging, we evaluated the autophagy levels of macrophages from the neoateries of the aging and young groups. TEM images showed the typical autophagosomes in homing cells of young group, while few autophagosome could be detected in the homing cells of aging group (Fig. S2a). Meanwhile, macrophages from the native arteries and neoarteries in aging and young groups were isolated via flow cytometric sorting. The purity of $CD68^+$ macrophages could be 90% and even higher (Fig. S2b). Subsequently, the LC3 protein levels of sorted macrophages were detected by WB. As shown in Fig. S2c, LC3II/I in neoarteries of aging group was significantly reduced as compared with that in young group at 2 weeks (Figs. S2c and d). Furthermore, we also detected the p62 protein levels of the sorted macrophages. P62 is considered to be a substrate in autophagic degradation, and the activation of autophagy usually causes a decrease in the p62 level [35]. Western blot confirmed that p62 expression of neoarteries in aging group was significantly up-regulated as compared with that in young group at 2 weeks (Figs. S2c and e). Taken together, aging may compromise autophagy in recruited macrophages in vascular grafts.

Besides, the polarization of macrophages was analyzed by iNOS/CD68 and CD206/CD68 co-immunofluorescence staining. As shown in Fig. S2f, the ratio of iNOS+/CD68+ cells significantly increased as compared with that in young group, while the ratio of CD206+/CD68+ cells was decreased (Figs. S2f and g). The predominant proportion of iNOS positive (pro-inflammatory) macrophages in aging group indicated an exacerbated pro-inflammatory polarization of macrophages at 2 weeks (Figs. S2f and g). These results suggested a positive correlation between decreased macrophage autophagy upon aging and pro-inflammatory polarization of macrophages.

3.3. The PGS-sodium citrate scaffold provides a stable drug-released platform for fast-degrading vascular grafts

The PGS-PCL grafts is composed of a PGS-salt mixing tube and an ultrathin electrospun sheath wrapping outside. In order to obtain appropriate drug loading efficiency and antithrombogenicity, sodium citrate was used instead of NaCl during the preparation of PGS-salt mixing tube. Owing to the anticoagulant effect of sodium citrate, grafts in sodium citrate group were treated without any water immersion procedure including salt leaching and heparinization (Fig. 1a). After nebulization treatment for 1 min, the sodium citrate incorporated vascular graft acquire adequate elasticity, which was conducive to suturing (Fig. 1b and c). As shown in Fig. 1d, grafts in sodium citrate group exhibited a sustained-release profile compared with NaCl group (Fig. 1d). The cumulative release reached 45.72 ± 8.69% of the total loading amount in sodium citrate group, whereas much lower releasing profile presented in NaCl group (11.06 ± 2.68% of the total loading amount). The cross-sections and outer surface of sheath examined by SEM revealed the porous PGS and the partial degradation of the collagen fibers (Diameter: 310 ± 98 nm) in the grafts of NaCl group (Fig. 1e). In contrast, grafts without water immersion (Fig. 1f) procedure contained a large number of sodium citrate particles and clearly identified collagen nanofibers (Diameter: 510 ± 77 nm) (see Fig. 1i).

Atomic force microscopy (AFM) revealed the surface roughness of grafts in NaCl group significantly decreased as compared with the sodium citrate group (Fig. 1g, h, i). Due to the filling of dissolving collagen

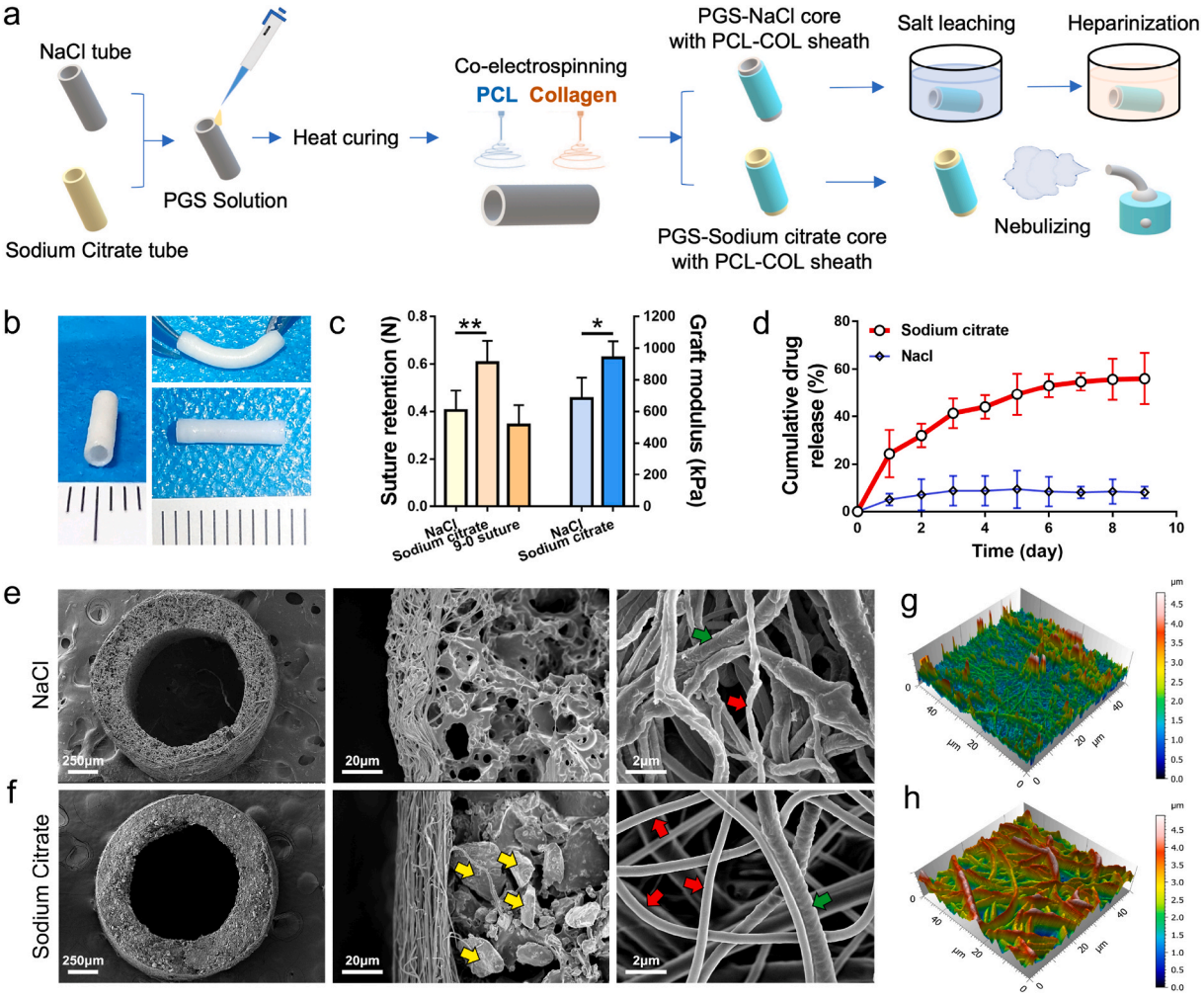

Parameters	Porous PGS Thickness (μm)	Sheath Thickness(μm)	Sheath surface Roughness(μm)	PCL fiber (nm)	Collagen fiber (nm)
NaCl	247.12±23.66	19.41±3.17	3.97±0.41	1170±109	310±98
Sodium citrate	258.91±18.27	22.07±1.79	4.89±0.17	1050±131	510±77

Fig. 1. Comparison of NaCl and sodium citrate in vascular grafts fabrication. **(a)** Schematic illustration for the fabricating process of vascular grafts. **(b)** Photographs of sodium citrate incorporated PCL/Col-PGS grafts after 1 min nebulizing. **(c)** Suture retention and elastic moduli of grafts. (PGS-NaCl core with PCL-Col sheath after 24 h salt leaching vs. PGS-Sodium citrate core with PCL-Col sheath after 1 min nebulizing, n = 5 independent samples). **(d)** Releasing profile of drug from grafts in sodium citrate group (red) and NaCl group (blue) (n = 3 independent samples). **(e, f)** SEM images showed the cross sections, detailed microstructure and PCL/Col fibers distribution of grafts in two groups. Yellow arrows mark the sodium citrate particles. Red arrows mark the collagen fibers. Green arrows mark the PCL fibers. **(g, h)** 3D images show the surface roughness of sheathes from NaCl group (**f**) and sodium citrate group (**g**) through atomic force microscopy (AFM). (**i**) The structural parameters of these two grafts were summarized (n = 5 independent samples). Data was presented as the mean ± SD for each group. For **c**, significance was determined by student t-test. *: $p < 0.05$, **: $p < 0.01$.

fibers, the surface of grafts in NaCl group appeared smoother thus reduces the contacting area on perivascular tissues, which may limit the effects of the drug. Notably, the presence of sodium citrate avoided disruption of collagen fibers and eliminated drugs loss during preparation, therefore provided a suitable drug-loaded platform for the fast-degrading vascular grafts.

3.4. GFP + macrophages ameliorated the potential of vascular regeneration after macrophage depletion

In our previous study, we constructed a peptide-loaded PCL sheath to modulate the polarization of macrophages, thereby improving vascular remodeling. During the limited peptide release time, a substantial infiltration of perivascular adipose (PVAT)-derived macrophages was observed in the PCL sheath [5]. We supposed that PVAT-derived macrophages are the indispensable mediators between pharmacological manipulation and vascular remodeling. To verify aforementioned speculation, rapamycin loaded vascular grafts were implanted in aging rats after depleting PVAT-derived macrophages. First, we tested the efficiency of depletion via comparing the number of recruited macrophages in Rapa loaded grafts after PBS and clodronate injection at two weeks post-implantation (Fig. S3). Results of CD68 immunostaining

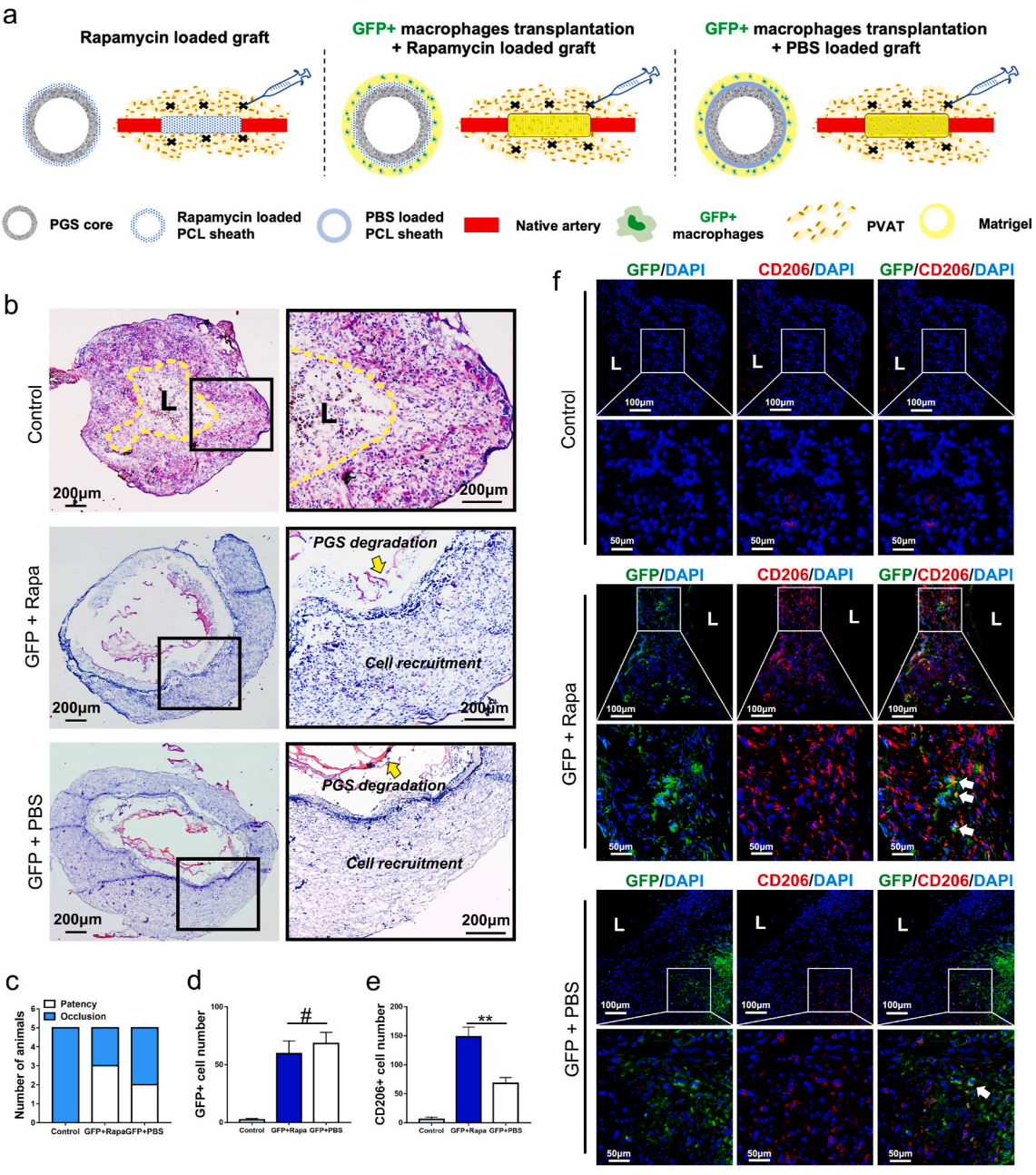

Fig. 2. GFP + Macrophages ameliorated the potential of vascular regeneration after macrophage depletion. (a) Schematic illustration of macrophage depletion via clodronate injection and GFP + macrophages transplantation in three groups. **(b)** HE staining of grafts from control, GFP + Rapa and GFP + PBS groups at 2 weeks postoperatively. **(c)** Comparing patency rates of control, GFP + Rapa and GFP + PBS groups at 2 weeks post-implantation (n = 5 independent samples). **(d, e)** Quantification of GFP + cells and CD206+ cells in neoarteries of control, GFP + Rapa and GFP + PBS groups at 2 weeks post-implantation. **(f)** Representative immunofluorescence images of neoarteries show CD206/GFP-double-positive cells in control, GFP + Rapa and GFP + PBS groups at 2 weeks post-implantation. DAPI was used to counterstain the nuclei. L: lumen. Data was presented as the mean ± SD for each group. For **d**, **e**, significance was determined by student t-test. #: $p > 0.05$, **: $p < 0.01$.

showed the number of macrophages in Rapa loaded grafts after clodronate injection was significantly decreased as compared with Rapa loaded grafts after PBS injection ($p < 0.01$), which confirms the validity of clodronate injection.

Given the pivotal roles of macrophages in vascular remodeling, we sought to transplant GFP + macrophages on PBS or rapamycin loaded graft after macrophages depletion. Matrigel containing GFP + macrophages were applied around the adventitia of PBS or rapamycin loaded vascular grafts respectively (Fig. 2a). Two weeks later, HE staining of the explants revealed collapsed lumens with irregular cellular arrangement suggested inappropriate vascular remodeling in control group (Fig. 2b). Five occluded grafts in the control group claimed the irreplaceable role of PVAT-derived macrophages in pharmacologically manipulated vascular remodeling (Fig. 2c). Surprisingly, the patency rate of rapamycin loaded graft reached 60% (3/5) after transplanting GFP + macrophages, which was significantly higher than that of control group (0%, 0/5) (Fig. 2c). Meanwhile, neoarteries in "GFP + macrophages" transplanting group (GFP + Rapa and GFP + PBS) presented normal cell recruitment and routine PGS degradation at 2 weeks (Fig. 2b). Immunofluorescence staining showed no difference between GFP + Rapa group and GFP + PBS group in the amount of recruiting GFP + macrophages (Fig. 2d and f, $p < 0.05$). Massive GFP-expressing macrophages were positive for CD206 in GFP + Rapa group, indicating the anti-inflammatory polarization of the transplanted macrophages at 2 weeks (Fig. 2e and f). Furthermore, the number of CD206+ anti-inflammatory macrophages in GFP + Rapa group was much higher than GFP + PBS group. These results suggested that loading rapamycin did not affect macrophages recruitment, while significantly promoted the anti-inflammatory polarization of recruited macrophages.

3.5. The evaluation of pharmacological manipulation of macrophage autophagy

To examine the autophagic influx in cells migrating into vascular grafts, co-immunostaining of CD68, vWF, a-SMA and CD3 respectively with LC3 was performed in harvested grafts at 2 weeks postoperatively. Obviously, LC3 was positively detected in PBS and Rapa groups, while 3-MA significantly inhibited its expression (Fig. 3a, d, g). Rapa group presented the higher ratio of LC3 positive cells as compared with PBS group, suggesting promoting role of loaded Rapamycin in autophagy of homing cells (Fig. 3c, i). Co-immunostaining of LC3 with CD68, vWF, a-SMA and CD3 respectively further revealed identity of cells in which autophagy were induced (Fig. 3a, d, g). Interestingly, LC3 positive cells were predominantly $CD68^+$ macrophages, cell counting and analysis suggested 42.61 ± 9.88% of $CD68^+$ macrophages were LC3+ (Fig. 3b and c). In contrast, few vWF + endothelial cells, $CD3^+$ T cells and only minority (8.34 ± 4.91%) of α-SMA + cells were positively stained with LC3 (Fig. 3c, f, i and Figs. S4a–c). This finding suggested that the macrophages are the main effector of Rapamycin, and autophagy was predominantly occurred in macrophages. The macrophage ratio in the neoarteries were further assessed by flow cytometry. No significant difference appeared among three groups in ratio of macrophage (Figs. S5a and b, $p > 0.05$). The results of flow cytometric analysis showed that over 90% of the cells were macrophages after separation (Figs. S5c and d). The isolated macrophages from digested tissues were collected for identifying markers involving in autophagy through Western blot. Western blot confirmed that p62 expression of macrophages in the 3-MA was significantly up-regulated as compared with that in the PBS group at 2 weeks, while it was obviously down-regulated in Rapa group (Figs. S5e and f). Meanwhile, LC3 protein and autophagy-related protein 5 (ATG5) are autophagosomes markers, and both of them exhibited up-regulated expression in the Rapa group (Figs. S5e, g, h). In contrast, LC3-II/LC3-I and ATG5 levels decreased significantly in the 3-MA group (Figs. S5e, g, h). LC3-II/LC3-I levels in the Rapa group elevated following downregulation of p-mTOR levels, confirming that rapamycin positively regulated autophagy through inhibiting mTOR (Figs. S5e and i).

In order to verify the pharmacological manipulation of macrophage autophagy in vitro, rat bone-marrow derived macrophages were seeded on PBS, rapamycin and 3-MA loaded scaffolds, respectively. TEM images showed the typical autophagosome formation in macrophages seeded in PBS and Rapa groups, while no autophagosomes formed in macrophages from 3-MA group (Fig. 4a). Immunofluorescent staining of LC3 showed the green fluorescence signals were mainly distributed in the nuclear regions of the PBS and 3-MA groups (Fig. 4b). In contrast, macrophages in the rapamycin group exhibited intense LC3 signals in the cytoplasm (Fig. 4b). Translocation of LC3 from the nucleus to the cytoplasm indicates activation of autophagy [36]. Furthermore, we used a tandem fluorescence mRFP-GFP-LC3 reporter system to monitor the autophagic flux in macrophages being seeded on the three drug-loaded scaffolds (Fig. 4c). Consistent with the data acquired from the in vivo study, the marked increase of both autophagosomes and autolysosomes was presented in macrophages seeded on Rapa grafts. (Fig. 4c and d). In contrast, both autophagosomes and autolysosomes in macrophages on 3-MA grafts significantly decreased. Western blotting was performed to compare autophagy-related protein levels among three groups. As expected, LC3-II/LC3-I level of macrophages from Rapa group was significantly increased as compared with PBS group (Fig. 4e and f). In addition, the utilization of 3-MA significantly reduced LC3-II/LC3-I level in macrophages (Fig. 4e and f). These results confirmed the efficacy of drug-loaded scaffolds in manipulating macrophage autophagy in vitro.

It has been reported that autophagy may facilitate cell survival in adverse microenvironments, such as inflammation and hypoxia, and inhibiting autophagy may promote apoptosis [37]. Considering the closely relationship between autophagy and apoptosis, we further examine the apoptosis of macrophages seeded into the different scaffolds (PBS, Rapa and 3-MA). Flow cytometry assay showed the apoptotic rates of macrophages in Rapa group were 3.87 ± 0.89%, which was not statistically different with PBS group (3.28 ± 1.09%, $p > 0.05$) (Figs. S6a and b). In contrast, apoptotic rate in 3-MA group (6.41 ± 1.37%) appeared significantly increased as compared with the other groups ($p < 0.05$) (Figs. S6a and b). These results suggested that autophagy induced by the released rapamycin less influenced the macrophage apoptosis, while 3-MA administration may increase the macrophage apoptosis.

3.6. Pharmacological manipulation of macrophage autophagy modulates the degradation of vascular grafts

To investigate the effect of modulating macrophage autophagy on in-vivo material degradation, we analyzed the harvested neoarteries of PBS, Rapa, and 3-MA loaded grafts at 2 weeks and 6 months after implantation. HE staining for slides from "2 weeks" time-point revealed that porous PGS almost degraded in PBS and Rapa group (PBS vs Rapa: 16.12 ± 3.67% vs 14.89 ± 2.01%, $p > 0.05$), which was consistent with our previous studies [8]. Interestingly, degradation of PGS graft was significantly delayed in 3-MA group, circular PGS residue was visible and occupied luminal part of the graft (Fig. 5a, c). According to the reported methods, polarized light images were used to visualize the distribution of PCL fibers [38–40]. The messy, loose bright fibers were frequently observed in remodeling PBS graft, which was consistent with the poor tissue remodeling in this group (Fig. 5b). In contrast, compactly and circularly arranged PCL fibers were observed in Rapa and 3-MA groups, while no significant difference was detected in degradation of PCL sheath among three groups (Fig. 5d, $p > 0.05$). Through 6 months, PGS has completely degraded in all groups (Fig. 5e, g), PCL sheath in all groups progressively degraded, and only about 3% of original PCL sheath remain visible in PBS and Rapa groups (Fig. 5f, h). In contrast, 3-MA slightly compromised PCL degradation through 6 months, which resulted in the 12.36 ± 3.17% of PCL residue (Fig. 5f, h). These results indicated that the inhibition of macrophage autophagy obviously delayed the in-vivo material degradation.

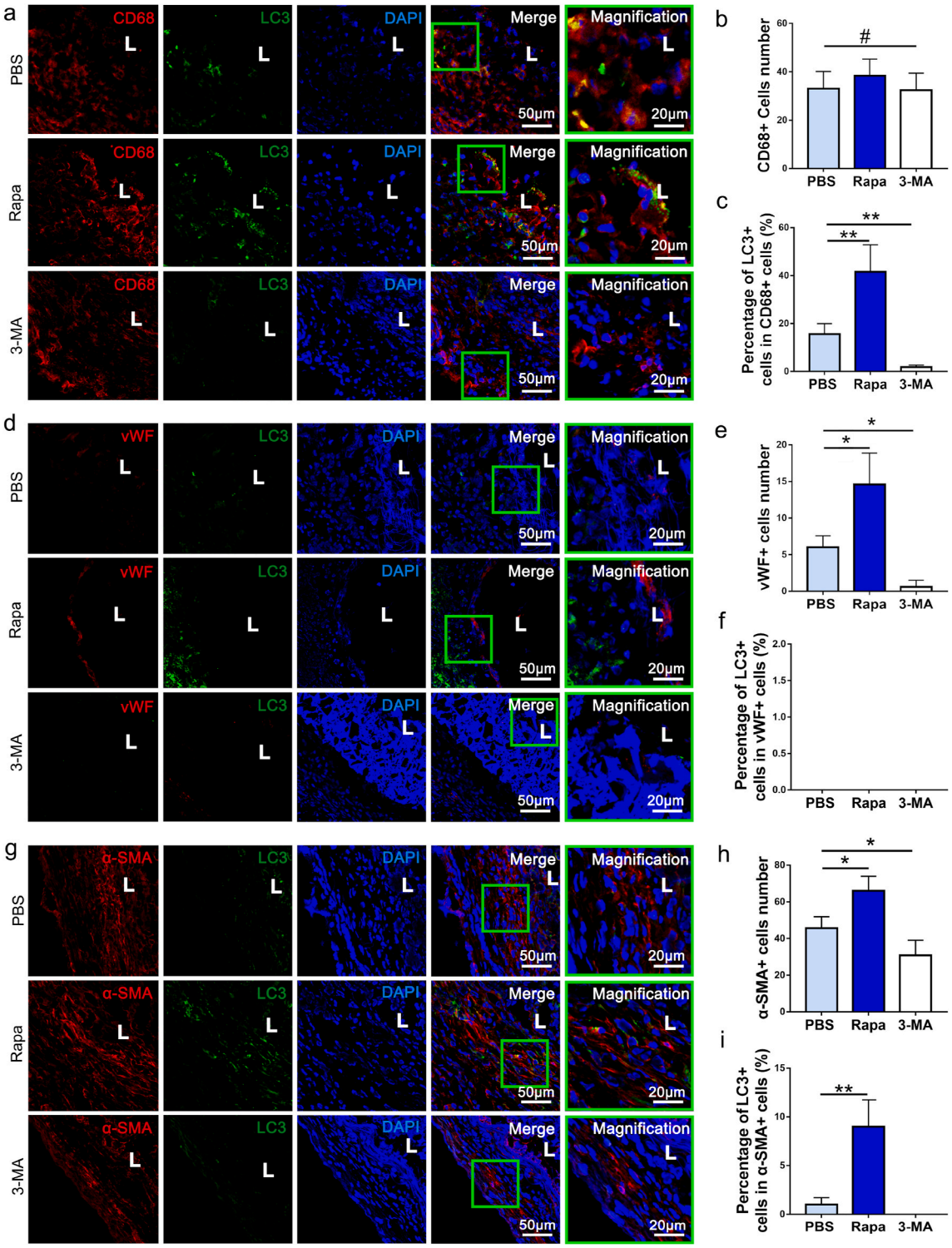

Fig. 3. The autophagic influx in cells migrating into vascular grafts. (a) Representative immunofluorescent co-staining of LC3 and CD68 in neo-arteries of PBS, Rapa and 3-MA groups at 2 weeks postoperatively. **(b)** Quantification of $CD68^+$ cells in PBS, Rapa and 3-MA groups respectively at 2 weeks (n = 3 independent samples). **(c)** The percentage of LC3+/CD68+ cells in all $CD68^+$ cells was calculated and compared among PBS, Rapa and 3-MA groups at 2 weeks (n = 3 independent samples). **(d)** Representative images showing immunofluorescent co-staining of LC3 and vWF in neoarteries of PBS, Rapa and 3-MA groups at 2 weeks. **(e)** Quantification of vWF + cells in PBS, Rapa and 3-MA group respectively at 2 weeks (n = 3 independent samples). **(f)** The percentage of LC3+/vWF + cells in PBS, Rapa and 3-MA grafts respectively at 2 weeks (n = 3 independent samples). **(g)** Representative images showing immunofluorescent co-staining of LC3 and α-SMA in neoarteries in PBS, Rapa and 3-MA groups at 2 weeks. **(h)** Quantification of α-SMA + cells in PBS, Rapa and 3-MA groups at 2 weeks (n = 3 independent samples). **(i)** The percentage of α-SMA+/LC3+ cells in PBS, Rapa and 3-MA groups at 2 weeks (n = 3 independent samples). L: lumen. DAPI was used to counterstain the nuclei. Data was presented as the mean ± SD for each group. For **b**, **c**, **e**, **f**, **h**, **i**, significance was determined by one-way ANOVA followed by Tukey's post hoc analysis. #: $p > 0.05$, *: $p < 0.05$, **: $p < 0.01$.

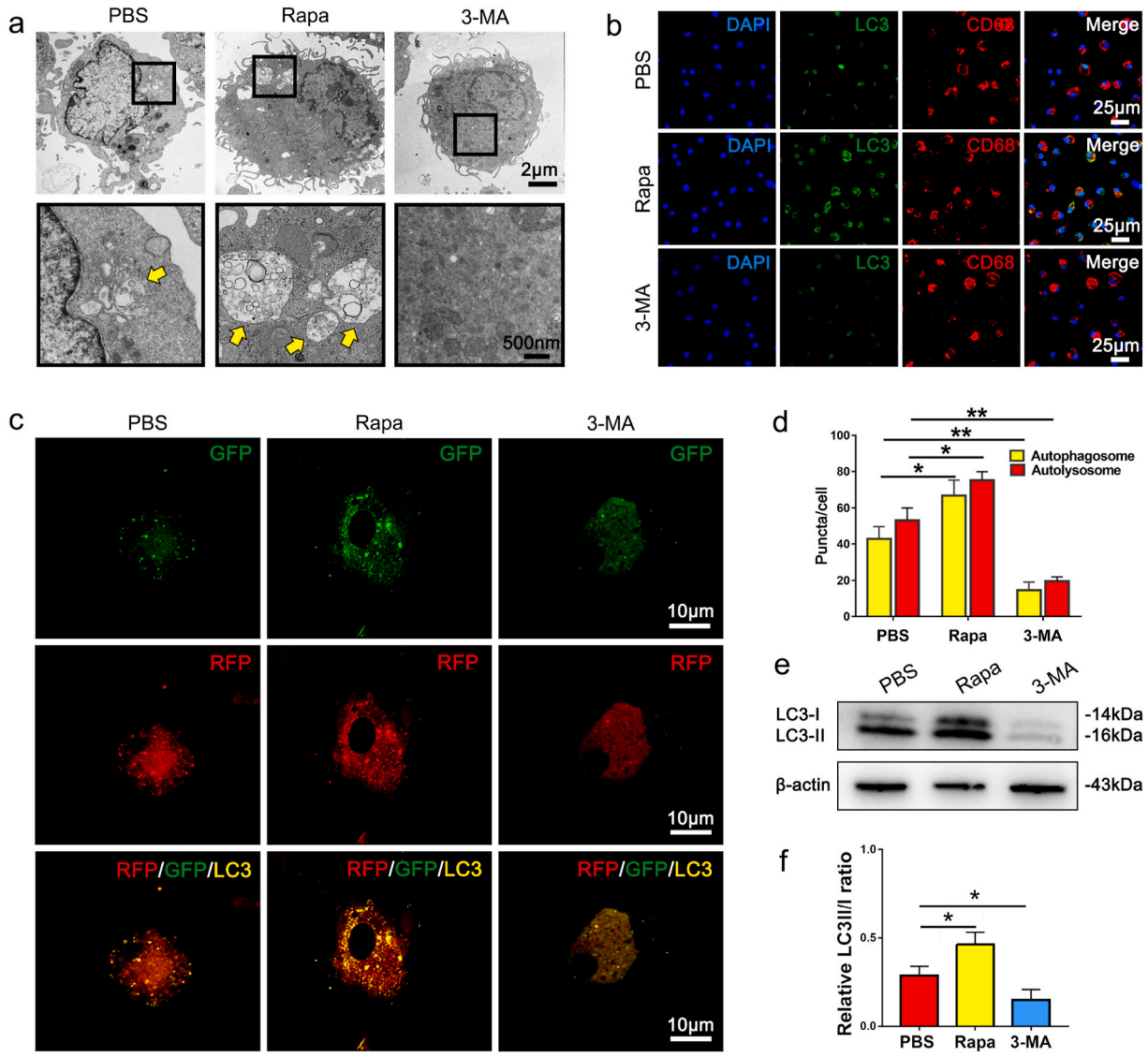

Fig. 4. In vitro evaluation of autophagy in macrophages seeded on PBS, Rapa and 3-MA loaded scaffolds. (a) TEM examination of macrophages seeded on PBS, Rapa and 3-MA scaffolds. Yellow arrows mark the autophagosomes. **(b)** Immunofluorescent staining of $CD68^{+}$ (red) macrophages with LC3 (green), and nuclei (blue) after 12 h' culturing on PBS, Rapa or 3-MA loaded scaffolds. **(c)** Laser confocal images showing the colocalization of some autophagosomes (yellow) and autolysosomes (red) in macrophages seeding in PBS, Rapa and 3-MA scaffolds. **(d)** Quantification of autophagosomes and autolysosomes in **c**. **(e)** Western blotting of LC3 expression in macrophages after 12 h' culturing on PBS, Rapa or 3-MA loaded scaffolds. (n = 3 independent samples). **(f)** Quantification of LC3-II/LC3-I in **e**. Data was presented as the mean ± SD for each group. For **d** and **f**, significance was determined by one-way ANOVA followed by Tukey's post hoc analysis. *: $p < 0.05$, **: $p < 0.01$.

3.7. Pharmacological manipulation of macrophage autophagy alters the macrophage inflammatory phenotype

To investigate the effect of modulating macrophage autophagy on macrophages polarization, we analyzed the polarization of macrophages seeded in PBS, Rapa and 3-MA loaded grafts in vitro (Fig. 6a). Immunofluorescence staining revealed the predominant proportion of CD206+ macrophages in Rapa loaded scaffolds, indicating the anti-inflammatory responses (Fig. 6b, d). Meanwhile, more than 80% macrophages in 3-MA loaded scaffolds were iNOS+, indicating typical pro-inflammatory transition. The similar trend was showed in the homing macrophages of PBS, Rapa and 3-MA loaded grafts in vivo. Immunofluorescent results showed a predominant proportion of iNOS+ (pro-inflammatory) macrophages in the 3-MA group, while majority of macrophages in the rapamycin-incorporated grafts presented typical anti-inflammatory transitions at 2 weeks (Fig. 6e and f). The findings suggested that the activation of autophagy promotes the anti-inflammatory polarization of macrophages while impaired autophagy promotes pro-inflammatory polarization of macrophages.

Trehalose is well-known as mTOR-independent autophagy inducer. To examine the direct effect of autophagy on polarization of anti-inflammatory macrophage, trehalose was loaded on the graft and cocultured with macrophages. Representative images of GFP-LC3 and RFP-LC3 fluorescence staining showed autophagosomes and autolysosomes in macrophages seeded on the trehalose loaded graft, which was significantly increased as compared with the PBS group ($p < 0.05$) (Figs. S7a and b). Furthermore, the number of autophagosomes in trehalose group was slightly lower than that in the Rapa group, which suggests a lower autophagy level. We further examined whether trehalose influenced macrophage polarization toward the anti-inflammatory phenotype. Immunofluorescence results showed the proportions of CD206+ macrophages in trehalose group were much higher than that in the PBS group (61.39 ± 7.91%, $p < 0.05$), while lower than that in the Rapa group ($p < 0.05$) (Figs. S7c–e). Next, 3 trehalose loaded vascular

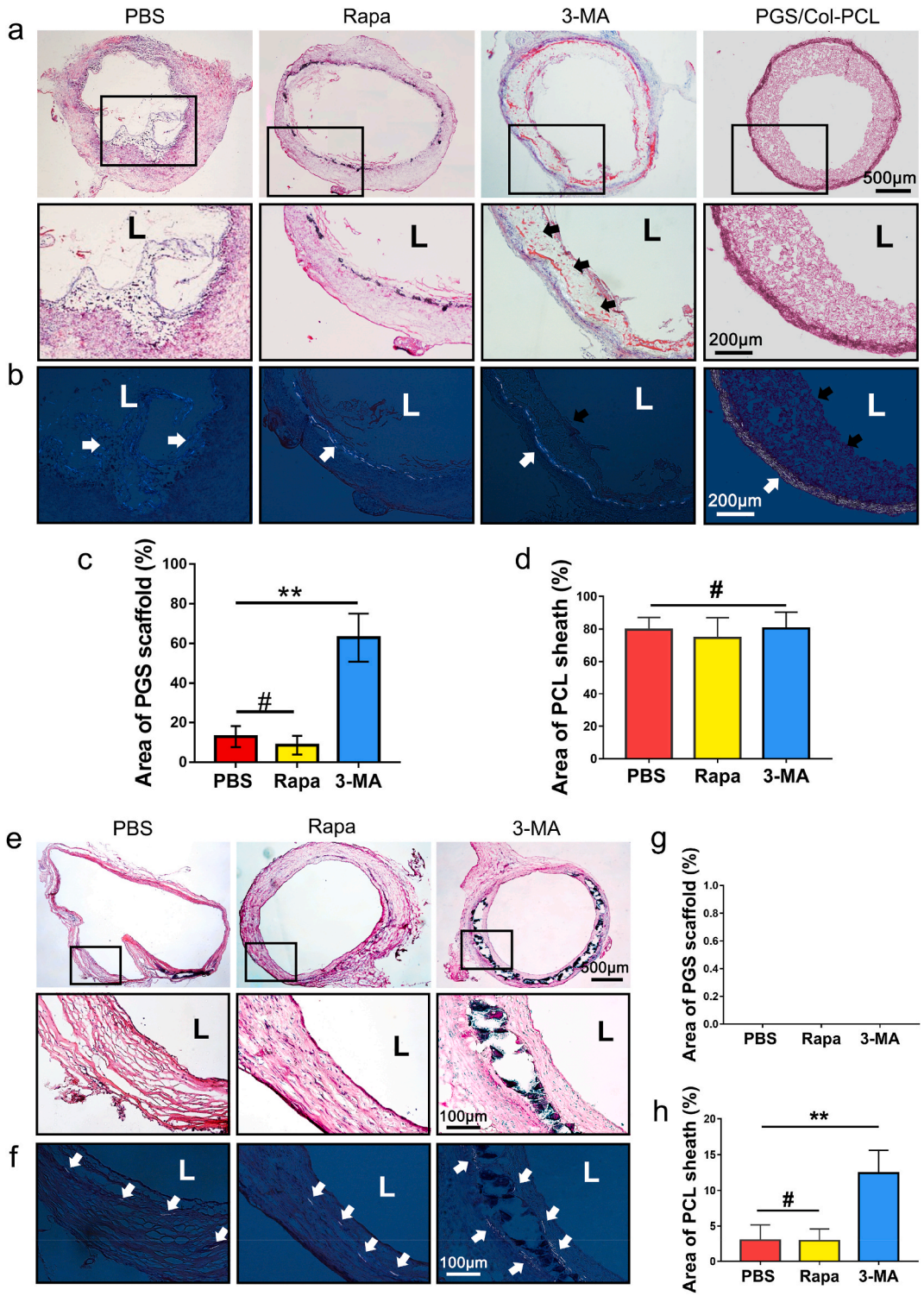

Fig. 5. Pharmacological manipulation of macrophage autophagy modulates grafts' degradation. (a) H&E staining of the neoarteries in PBS, Rapa and 3-MA groups at 2 weeks postoperatively, original PGS-PCL graft as control. Black arrows mark the region of residual PGS scaffold. **(b)** Polarized light images from the neoarteries in PBS, Rapa and 3-MA groups at 2 weeks, and original PGS-PCL graft. White arrows mark the region of residual PCL scaffold. **(e)** H&E staining of the neoarteries in PBS, Rapa and 3-MA groups at 6 months postoperatively. Black arrows mark the region of residual PGS scaffold. **(f)** Polarized light images from the neoarteries in PBS, Rapa and 3-MA groups at 6 months postoperatively. White arrows mark the region of residual PCL sheath. **(c, d, g, h)** Quantitative comparison of the residual PGS, and PCL sheath area (%) (residual area/total area before implantation) among different groups. Area was identified and quantified from H&E staining and polarized images. L: lumen. Data was presented as the mean ± SD for each group. For **c**, **d**, **g**, **h**, significance was determined by one-way ANOVA followed by Tukey's post hoc analysis. #: $p > 0.05$, **: $p < 0.01$.

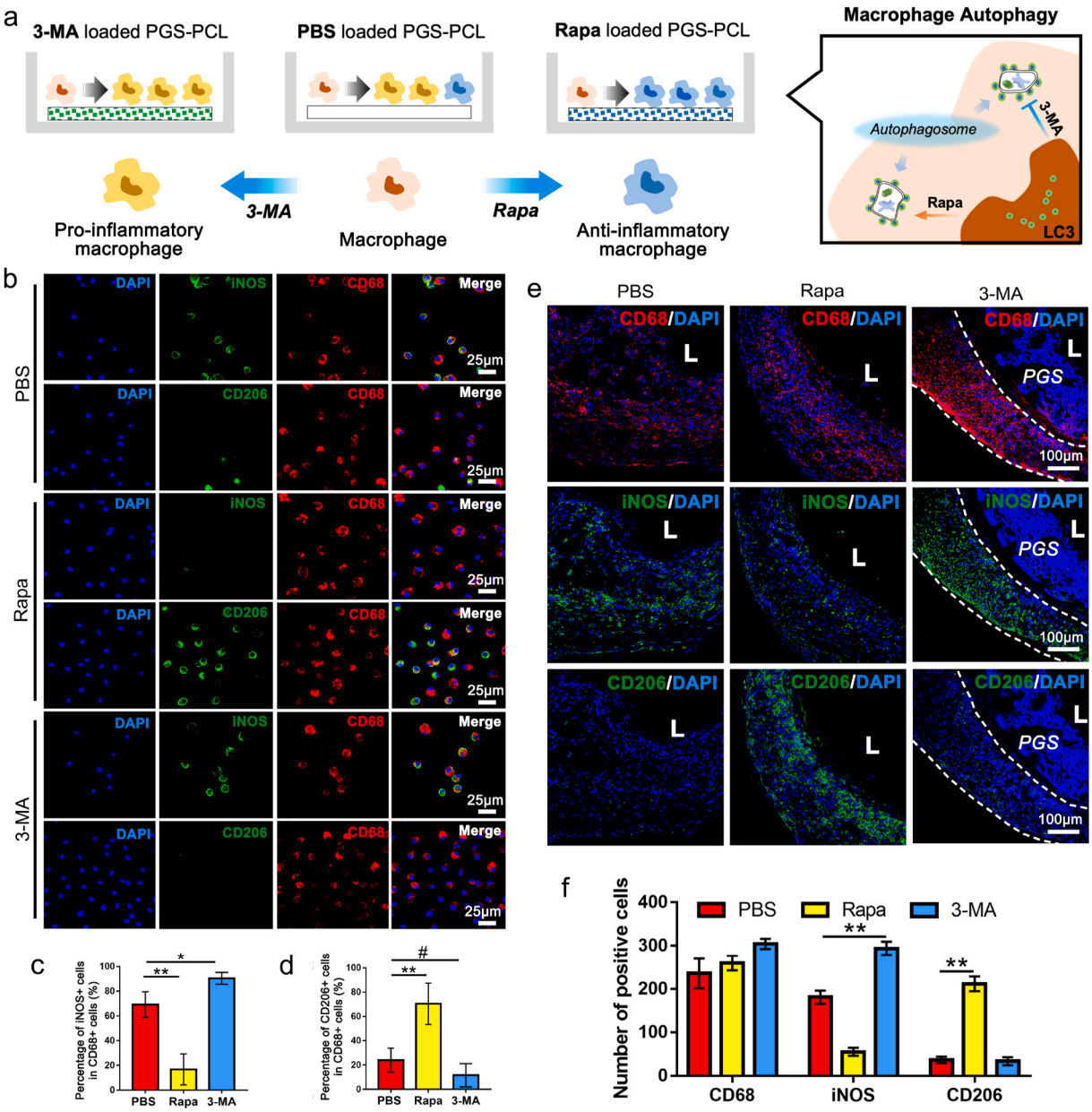

Fig. 6. Pharmacological manipulation of macrophage autophagy modulates the polarization of macrophages. (a) Schematic illustration of polarization of macrophages seeded on PBS, Rapa and 3-MA loaded scaffolds. **(b)** Immunofluorescence staining of CD68 (red), iNOS (green) and CD206 (green) in macrophages seeded on PBS, Rapa or 3-MA loaded scaffolds. **(c, d)** Quantification of iNOS+/CD68+ cells and CD206+/CD68+ cells in macrophages seeded in PBS, Rapa and 3-MA loaded scaffolds (n = 3 independent samples). **(e)** Representative immunofluorescent staining of iNOS, CD206 and CD68 in neoarteries of PBS, Rapa and 3-MA loaded grafts at 2 weeks post-implantation. **(f)** Quantification of $CD68^{+}$, iNOS+ and CD206+ cells in PBS, Rapa and 3-MA loaded grafts respectively at 2 weeks post-implantation. (n = 3 independent samples). L: lumen. Data was presented as the mean ± SD for each group. For **c**, **d**, **f**, significance was determined by one-way ANOVA followed by Tukey's post hoc analysis. #: $p > 0.05$, **: $p < 0.01$.

grafts were implanted in the arteries of aging rat. At 2 weeks after implantation, 2 grafts were patent (Figs. S7f and g). As immunofluorescence staining shown, macrophages in the neoarteries of trehalose groups presented dominant proportion of CD206+ subset (iNOS vs CD206: 32.17 ± 4.13 vs 59.69 ± 7.92%) and suggesting the anti-proinflammatory polarization (Figs. S7h and i). These results further confirmed that the activation of autophagy promotes the anti-inflammatory polarization of macrophages.

3.8. Pharmacological manipulation of macrophage autophagy modulates endothelial coverage of vascular graft

In order to present the endothelial coverage on different sites (suture site, quarter site and mid site), frozen longitudinal sections of neoarteries in PBS, Rapa and 3-MA groups at 2 weeks postoperatively were used for vWF immunofluorescence staining. As shown in Fig. 7a–d, the EC coverage at suture site in Rapa group (90.84 ± 6.67%) was similar to PBS group (92.61 ± 7.09%, $p > 0.05$), while EC coverages on the quarter and mid regions the of Rapa graft were both significantly increased as compared with the controls (quarter site: 81.91 ± 9.82% vs 58.62 ± 10.11%, mid site: 76.83 ± 9.54% vs 43.77 ± 11.85%, $p < 0.05$). ECs from the autologous blood vessels at both ends of the graft can proliferate and migrate to the luminal surface of graft, therefore the EC coverage on suture sites was not statistically different between Rapa and PBS group (Fig. 7b). However, Rapa grafts presented significant increased ECs coverage in the other two sites, indicating that adequately

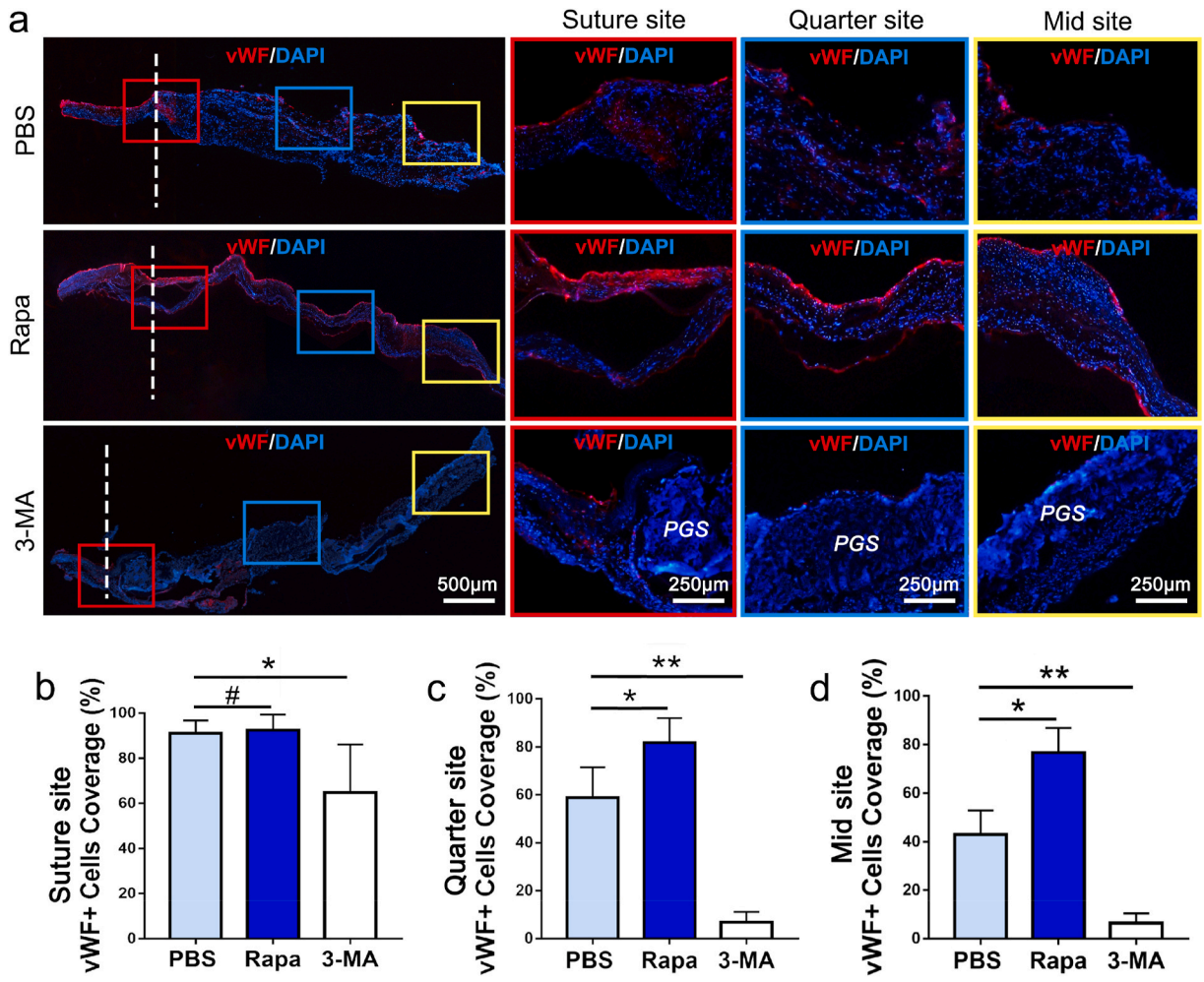

Fig. 7. Longitudinal views on EC coverage of neoarteries in PBS, Rapa and 3-MA groups at 2 weeks postoperatively. (a) Immunofluorescent staining for vWF-positive cells on longitudinal sections of neoarteries in three groups. **(b–d)** Quantification of endothelial coverage by determining the percentage of vWF positive region from total luminal length at suture, quarter and mid sites (n = 3 independent samples). DAPI was used to counterstain the nuclei. Data was presented as the mean ± SD for each group. For **b**, **c**, **d**, significance was determined by one-way ANOVA followed by Tukey's post hoc analysis. #: $p > 0.05$, *: $p < 0.05$, **: $p < 0.01$.

elevated macrophage autophagy was beneficial to graft's endothelialization (Fig. 7c and d). Different from Rapa and PBS group, in the luminal layer of 3-MA group, substantial remnants of the PGS material were visible (Fig. 7a). The compromised degradation induced by 3-MA resulted decreased ECs coverage at three sites as compared with the PBS group (suture site: 63.34 ± 11.79% vs 92.61 ± 7.09%, quarter site: 81.91 ± 9.82% vs 5.21 ± 1.76%, mid site: 4.37 ± 2.98% vs 43.77 ± 11.85%, $p < 0.05$) (Figure b–d).

3.9. *Pharmacological activation of macrophage autophagy effectively promotes long-term muscular remodeling of vascular grafts in aging bodies*

To examine the myogenic differentiation of homing progenitors in remodeling grafts, immunofluorescence staining and Western blot analysis against α-SMA and SM-MHC were performed. As shown in Fig. 8a, early recruitment of a-SMA + cells were detected predominantly at adventitial side of the Rapa loaded grafts at 2 weeks, while recruited a-SMA + cells were significantly reduced in PBS and 3-MA group, which suggested that Rapamycin may attenuate poor mobilization of myogenic cells in aging body (Fig. 8a–c). At 6 months, cells positively stained α-SMA and SM-MHC both increased in PBS loaded grafts and penetrated the whole vessel wall, although it was still fewer and sparser than that in Rapa loaded grafts (Fig. 8d–f). The 3-MA loaded grafts remain less myogenic through 6 months, as was characterized by scarce of a-SMA+ and SM-MHC + cells (Fig. 8d–f). Western blot analysis confirmed the trend revealed in immunofluorescent images, Rapamycin loaded in PGS-PCL grafts enhanced recruitment of myogenic cells at 2 weeks, and promoted differentiation into SMCs through 6 months (Fig. 8g-l). Fibrotic response of the grafts was also characterized by immunostaining with fibroblast surface protein (FSP) antibody. As shown in Figure 8m, FSP + cells increased significantly through 2 weeks to 6 months, especially in PBS and 3-MA groups. These cells distributed in adventitia layer as well as on luminal side, suggesting the trend of vessel wall fibrosis with aging. In contrast, the FSP + cells dramatically decreased in Rapa group, both at 2 weeks and 6 months, suggesting antifibrotic effect of Rapamycin in vascular grafts (Fig. 8m–o).

The long-term patency determined by necropsy was 87.50% (7/8) in Rapa group, which is much higher than that in PBS group (62.5%, 5/8) (Fig. S8g). However, the loading of 3-MA significantly decreased patency rate (37.5%, 3/8, Fig. S8g). H&E staining showed that a large amount of undegraded PCL remained in the lumens of 3-MA loaded grafts at 6 months (Fig. 3e). The undegraded material distributed evenly and formed a three-layer sandwich with extremely dense ECM fibers and less cellularization, which could be regarded as scar tissues encapsulate the residual materials (Fig. 3e). Immunofluorescence results confirmed that the main component in 3-MA loaded grafts was COL-I, one of the main constituents of scar tissue (Fig. S8e). Further "Alizarin red" staining revealed that ossification or calcification occurred in the vessel

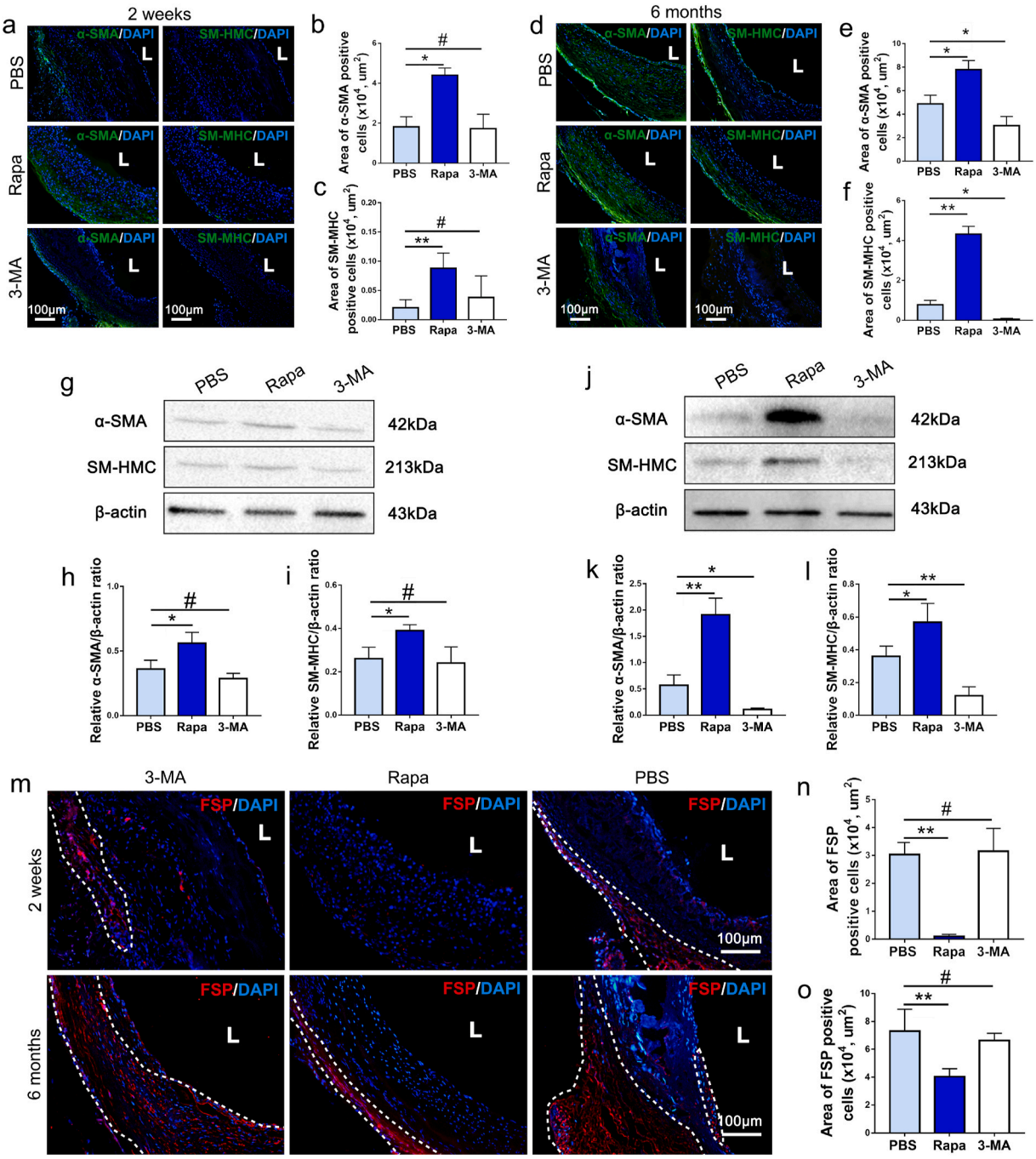

Fig. 8. Pharmacological activation of macrophage autophagy effectively promotes long-term muscular remodeling of vascular grafts in aging bodies. (a, d) The representative images of α-SMA and SM-MHC immunofluorescence staining for neoarteries in PBS, Rapa and 3-MA groups. DAPI was used to counterstain the nuclei. **(b, c, e, f)** Quantification of area of α-SMA+ and SM-MHC + cells in PBS, Rapa and 3-MA groups respectively at 2 weeks or 6 months post-implantation (n = 3 independent samples). **(g)** Expression of α-SMA and SM-MHC proteins in each group at 2 weeks was detected by Western blot. **(h, i)** Quantification of α-SMA and SM-MHC protein levels in each group at 2 weeks (n = 3 independent samples). **(j)** Expression of α-SMA and SM-MHC proteins in each group at 6 months was detected by Western blot. **(k, l)** Quantification of α-SMA and SM-MHC protein levels in each group at 6 months (n = 3 independent samples). **(m)** Fibroblast surface protein (FSP, red) positive cells were sparsely distributed in the outermost layer of the vessel wall, which was marked with white dots line. **(n, o)** Statistical analysis of FSP + cells at high magnification images were performed, which showed Rapamycin effectively reduced fibrosis in vascular graft in aging body (n = 3). DAPI was used to counterstain the nuclei. L: lumen. Data was presented as the mean ± SEM for each group. For **b**, **c**, **e**, **f**, **h**, **I**, **k**, **l**, **n**, **o**, significance was determined by one-way ANOVA followed by Tukey's post hoc analysis. #: $p > 0.05$, *: $p < 0.05$, **: $p < 0.01$.

walls of 3-MA loaded grafts (Fig. S8c), which shared the same location with the residual PCL (Fig. 3e). In contrast to the adverse remodeling noted in the 3-MA group, histological examination presented significantly improved muscular remodeling in the Rapa group. Neoarteries in Rapa group presented a homogeneous, continuous muscular structure characterized by closely packed, regularly arranged collagen and elastic fibers (Figs. S8a–f). Immunofluorescent staining confirmed that appropriate amounts of collagen III and elastin, typical markers of muscular arteries, were the major components of ECM in the Rapa group (Figs. S8h–j). In addition, immunofluorescent staining and Western blot analysis of neoarteries harvested at 2 weeks presented significantly higher ratios of phospho-AMPK (p-AMPK) to AMPK in the Rapa group

than in the PBS group, while the 3-MA group exhibited a slightly lower p-AMPK/AMPK value than the PBS group (Figs. S9a–c). AMPK activation is an important representation of enhanced differentiation of myogenic stem cells [34]. The cellular AMPK activation in Rapa group at 2 weeks confirmed the crucial role of macrophage autophagy in initial muscular remodeling of graft. These findings indicated that administrating the autophagy activator rapamycin in vascular grafts rejuvenated endogenous elastin production from SMCs in aging individual, while the autophagy inhibitor 3-MA exacerbated graft fibrosis and calcification.

3.10. Pharmacological activation of macrophage autophagy promotes the myogenic differentiation of Sca-1+ stem cells in vitro

Macrophages, seeded on PBS, Rapa, and 3-MA incorporated scaffolds respectively, were cocultured with Sca-1+ stem cells (Fig. S10a). Myogenic differentiation of Sca-1+ stem cells was revealed by increasing numbers of SM-MHC + cells (Fig. S10a). Quantitatively, the number of SM-MHC positive cells was significantly higher in Rapa group than that in PBS group at 14 days, while few SM-MHC positive cells were observed in the 3-MA group (Figs. S10b and c). These results confirmed that myogenic differentiation of Sca-1+ stem cells could be effectively promoted through activating macrophage autophagy.

4. Discussion

Declining regenerative potential and aggravated inflammation upon aging create inappropriate environment for arterial regeneration. The decreased autophagy observed in aged macrophages contributes to their functional decline and aberrant inflammatory cytokine production [16]. It's known that impaired autophagy would guide pro-inflammatory polarization of macrophages [41], which was also observed in our study. Early infiltrating macrophages in grafts from aging group presented compromised autophagy and manifested a distinct pro-inflammatory phenotype with elevated iNOS + macrophages. The pro-inflammatory polarization of macrophages compromised the recruitment and differentiation of progenitor cells [42] and eventually leads to poor vascular remodeling. On the contrary, macrophage polarization towards anti-inflammatory phenotype attenuate inflammation and favored tissue regeneration [43]. Moderate activation of autophagy suppresses pro-inflammatory polarization, promotes anti-inflammatory polarization, and alleviates inflammatory reactions [44,45]. Therefore, constructing anti-inflammatory microenvironment via manipulating macrophages autophagy is expected to be an efficient approach to rescuing impaired vascular remodeling in aging body. To prove this, autophagy-targeting drugs rapamycin and 3-MA were loaded on the PCL sheath of the vascular grafts. As a result, activation of autophagy by rapamycin drives the polarization of macrophages towards an anti-inflammatory state and simultaneously amends the impaired vascular remodeling in aging bodies. Conversely, inhibition of autophagy by 3-MA aggravates the pro-inflammatory macrophage polarization in aging bodies and finally lead to severe arterial fibrosis and calcification. These results confirmed pivotal roles of macrophages autophagy in modulating the graft's immune microenvironment and offer alternative strategy for materials modification. Moreover, regulating the perivascular immune microenvironment significantly ameliorates aging induced defective regeneration. To the best of our knowledge, applying rapamycin as immunomodulatory agent to improve regenerative potential of aging body, is new to vascular substitutes.

The innate autophagic potential of macrophages is essential to the host remodeling of biodegradable materials. We have previously claimed that in vivo degradation of PGS is closely related to the recruited macrophages, but the concrete mechanism remains uncertain [5]. Interestingly, this study revealed that PGS degradation significantly delayed once 3-MA was loaded in PCL sheath, and autophagy of recruited macrophages was significantly suppressed. Phagocytosis and autophagy of macrophages are typically dedicated to degradation of substrates from extrinsic and intrinsic origins [46]. It was shown that macrophages lacking autophagy failed to degrade engulfed cargo [47], and produced macrophage migration inhibitory factors [48]. Macrophages-mediated material degradation is an energy consuming action while autophagy favors ATP provision in ischemic conditions [49]. For those macrophages pioneering the degradation of the porous PGS, adequate autophagy is essential to their survival in scaffolds. 3-MA, the inhibitor of cellular autophagy, disrupted the energy supply for macrophages and halted the recruitment of macrophages to PGS thus caused the delayed material degradation. Our study also revealed enhanced thrombosis inside PGS tube and decreased patency rate when 3-MA impeded PGS degradation. Combined with our previous studies, we failed to acquire the evidence that the endothelial cells could adhere on PGS lumen, while endothelialization was realized by adhesion of ECs on the luminal side of PCL sheath [8]. Timely degradation of PGS relying on macrophage autophagy is indispensable for the rapid endothelialization of PGS-PCL graft. Collectively, macrophage autophagy has been found manipulating grafts degradation in this study, which may be the new target for rational design of vascular grafts.

Prevalent strategies for improving host remodeling of vascular grafts are loading chemotaxis factors of vascular forming cells such as VEGF or peptides to improve ECs adhesion [50,51]. ECs proliferation, migration, and adhesion are known to be regulated through a complex signaling network [52]. The effect of loading single growth factor is rather limited. Our study confirmed extensive promoting roles of constructing anti-inflammatory microenvironment in accelerating endothelialization and improving muscular remodeling in aging body, which suggested superiority over the single effect of loading growth factors. The utilization of rapamycin increased the number of anti-inflammatory macrophages in the perivascular microenvironment via activating autophagy. Anti-inflammatory macrophages are proven to secrete multiple growth factors, such as VEGF, VEGF-C and -D, PDGF, and TGF-β [53,54], that meet the complex needs of endothelialization. As the result, the anti-inflammatory perivascular microenvironment created by rapamycin was conducive to rapid endothelialization of the graft and improved graft patency rate. In contrast, the utilization of 3-MA aggravated the pro-inflammatory polarization of macrophages in aging bodies. Several studies have demonstrated that IL-1 and transforming growth factor secreted by pro-inflammatory macrophages can destroy tight junctions of endothelial cells, and excessive secretion of IL-8 may impair endothelial tube growth [55,56]. Therefore, compromised endothelialization in the 3-MA group may be partly attributed to pro-inflammatory microenvironment. Furthermore, a large number of AMPK-activated cells were shown around the rapamycin loaded PCL sheath in aging bodies. AMPK activation is known to be an important feature of enhanced differentiation of myogenic stem cells [34]. In consistence with such dogma, six months in vivo results in present study revealed that neoarteries in rapamycin loaded grafts produced adequate amount of elastin and COL-III closing to native artery, and the incidence of aneurysms was significantly reduced. Recent studies suggest that age-related regenerative defects may result from miscommunication between immune cells and tissue stem cells, as well as an accumulation of proinflammatory mediators in the tissue [57]. The keys to reversing the aging process of stem cells and rejuvenating tissues will be therapies that not only stimulate tissue stem cell self-renewal but also target inflammatory mediators accumulating with age.

Vascular calcification, an irreversible pathologic change in aging vessels, is significantly aggravated in neo-artery when autophagy inhibitor 3-MA is loaded in grafts. Macrophage autophagy play a critical role in the degradation and recycling of long-lived/damaged intracellular material [58,59]. Inhibiting macrophage autophagy led to the overabundance of cellular debris and cytotoxic material, which is a paramount contribution to the exacerbated calcification. In our study, administrating rapamycin rejuvenated the senescent macrophages via

activating autophagy and significantly enhanced the clearance ability of macrophage to handle vascular calcification in aging bodies. Furthermore, progression of vascular calcification is closely related to macrophages [60], which is the dominant cells in immune microenvironments of PBS and 3-MA groups. Osteoblastic differentiation of vascular smooth muscle cells is a major event of vascular calcification [61], Chronic inflammation caused by pro-inflammatory macrophage impairs the normal development of VSMCs [62] and pro-inflammatory macrophage can directly release oncostatin M (OSM) to promote the differentiation of VSMCs into osteoblastic phenotypes [63]. Conversely, anti-inflammatory macrophage can inhibit the osteogenic conversion of VSMCs [64] and secrete anti-inflammatory factors as well as phagocytize necrotic fragments and apoptotic cells to prevent the formation of calcified nucleation sites [65]. Anti-inflammatory polarization activated by rapamycin created an anti-inflammatory microenvironment that effectively suppressed vascular calcification in aging bodies. Different from the limited success achieved to promote regeneration by directly loading the M2-type macrophage polarization factor like IL-4, the loading of autophagy inducer rapamycin comprehensively activates multiple necessary functions of macrophages involved in the regression of vascular calcification. This pro-regenerative microenvironment dominated by autophagy-activated macrophages provides long-lasting improvement in aging-induced defective regeneration, which may give new insights for rational design of vascular grafts in aging bodies.

As shown in our previous study, "perivascular adipose tissue (PVAT)-derived macrophages" has been identified as the main effector cells for the drug loaded on PCL sheath [5]. The recruitment of bone marrow-derived monocyte is an indispensable source for the supplement and accumulation of macrophages in adipose tissue, especially during inflammation [66,67]. The perivascular adipose tissue is rich in capillaries, which may enable the migration of circulating monocytes into the tissue around the vascular grafts. In this study, bone marrow derived GFP + macrophages efficiently recovered potential of vascular remodeling after original PVAT-macrophages were killed, therefore confirmed the major contribution of circulating macrophages in regeneration mediated by PVAT derived macrophages. According to the degradation patterns of PGS-PCL grafts, the degradation of PGS was mainly regulated by macrophages derived from circulating blood at the initial remodeling stage. When PGS layer completely degrade, PCL layer alone will restrict the infiltration of cells from circulating blood due to the compact fibril structure. Therefore, macrophages derived from PVAT are the main sources involving in long-term vascular remodeling around the PCL sheath. In order to efficiently act on the recruited macrophages from these two sources, we loaded the autophagy-regulated drugs in the collagen fiber of PCL/Col sheath. Electrospinning collagen may preserve molecular structure of drugs, avoid possible damage during covalent binding process. Moreover, the inclusion of collagen fibers in PCL nanofibers provided increased porosity and favored the adhesion and spreading of cells [5]. However, due to rapid degradation of collagen, the loaded drugs are quickly released within a short releasing period. To prolong the pharmacological effect, entrapping the drugs in liposomes should be explored in further study. Due to good biocompatibility and biodegradability, slow-release potential, and strong tissue affinity [68], liposomes may enable autophagy targeted drugs to exert long-term effects.

5. Conclusion

In this study, we successfully ameliorate aging induced compromised vascular regeneration through manipulating macrophage autophagy, and confirmed the roles of macrophage autophagy in degrading PGS/PCL grafts and anti-inflammatory macrophage polarization. Rapamycin was shown to hold the potential as a safe and potent agent for anti-inflammatory therapy of vascular grafts. Our work develops a new anti-inflammatory therapeutic strategy based on autophagy-induced anti-inflammatory polarization which may pave a new avenue for clinical translation of vascular grafts in aging bodies.

CRediT authorship contribution statement

Wanli Chen: Investigation, Formal analysis, Validation, Methodology, Writing – original draft, Writing – review & editing. **Weiwei Xiao:** Investigation, Formal analysis, Writing – review & editing. **Xuzheng Liu:** Investigation, Formal analysis, Writing – review & editing. **Pingping Yuan:** Investigation, Methodology. **Siqian Zhang:** Investigation. **Yinggang Wang:** Investigation. **Wei Wu:** Supervision, Conceptualization, Visualization, Validation, Writing – review & editing.

Acknowledgements

This project was financially supported by National Natural Science Foundation of China (No.82071132, 81422008, 81771040).

Appendix A. Supplementary data

Supplementary data to this article can be found online at https://doi.org/10.1016/j.bioactmat.2021.09.027.

Declaration of competing interest

We declare that we have no known competing financial interests or personal relationships that could have appeared to influence the work reported in this paper.

References

[1] D. Radke, W. Jia, D. Sharma, K. Fena, G. Wang, J. Goldman, F. Zhao, Tissue engineering at the blood-contacting surface: a review of challenges and strategies in vascular graft development, Advanced healthcare materials 7 (2018), e1701461, https://doi.org/10.1002/adhm.201701461.

[2] R. Nosalski, T.J. Guzik, Perivascular adipose tissue inflammation in vascular disease, Br. J. Pharmacol. 174 (2017) 3496–3513, https://doi.org/10.1111/bph.13705.

[3] W. Gu, W.N. Nowak, Y. Xie, A. Le Bras, Y. Hu, J. Deng, S. Issa Bhaloo, Y. Lu, H. Yuan, E. Fidanis, A. Saxena, T. Kanno, A.J. Mason, J. Dulak, J. Cai, Q. Xu, Non-lethal sonodynamic therapy facilitates the M1-to-M2 transition in advanced atherosclerotic plaques via activating the ROS-AMPK-mTORC1-autophagy pathway, Arterioscler. Thromb. Vasc. Biol. 39 (2019) 2049–2066, https://doi.org/10.1161/atvbaha.119.312732.

[4] P.J. Psaltis, R.D. Simari, Vascular wall progenitor cells in health and disease, Circ. Res. 116 (2015) 1392–1412, https://doi.org/10.1161/CIRCRESAHA.116.305368.

[5] W. Chen, S. Jia, X. Zhang, S. Zhang, H. Liu, X. Yang, C. Zhang, W. Wu, Dimeric thymosin β4 loaded nanofibrous interface enhanced regeneration of muscular artery in aging body through modulating perivascular adipose stem cell-macrophage interaction, Adv. Sci. 7 (2020) 1903307, https://doi.org/10.1002/advs.201903307.

[6] Y. Pan, J. Yang, Y. Wei, H. Wang, R. Jiao, A. Moraga, Z. Zhang, Y. Hu, D. Kong, Q. Xu, L. Zeng, Q. Zhao, Histone deacetylase 7-derived peptides play a vital role in vascular repair and regeneration, Adv. Sci. 5 (2018) 1800006, https://doi.org/10.1002/advs.201800006.

[7] J.D. Roh, R. Sawh-Martinez, M.P. Brennan, S.M. Jay, L. Devine, D.A. Rao, T. Yi, T. L. Mirensky, A. Nalbandian, B. Udelsman, N. Hibino, T. Shinoka, W.M. Saltzman, E. Snyder, T.R. Kyriakides, J.S. Pober, C.K. Breuer, Tissue-engineered vascular grafts transform into mature blood vessels via an inflammation-mediated process of vascular remodeling, Proc. Natl. Acad. Sci. U.S.A. 107 (2010) 4669–4674, https://doi.org/10.1073/pnas.0911465107.

[8] W. Wu, R.A. Allen, Y. Wang, Fast-degrading elastomer enables rapid remodeling of a cell-free synthetic graft into a neoartery, Nat. Med. 18 (2012) 1148–1153, https://doi.org/10.1038/nm.2821.

[9] K.W. Lee, P.S. Gade, L. Dong, Z. Zhang, A.M. Aral, J. Gao, X. Ding, C.E.T. Stowell, M.U. Nisar, K. Kim, D.P. Reinhardt, M.G. Solari, V.S. Gorantla, A.M. Robertson, Y. Wang, A biodegradable synthetic graft for small arteries matches the performance of autologous vein in rat carotid arteries, Biomaterials 181 (2018) 67–80, https://doi.org/10.1016/j.biomaterials.2018.07.037.

[10] X. Yang, J. Wei, D. Lei, Y. Liu, W. Wu, Appropriate density of PCL nano-fiber sheath promoted muscular remodeling of PGS/PCL grafts in arterial circulation, Biomaterials 88 (2016) 34–47, https://doi.org/10.1016/j.biomaterials.2016.02.026.

[11] F. Loi, L.A. Cordova, J. Pajarinen, T.H. Lin, Z. Yao, S.B. Goodman, Inflammation, fracture and bone repair, Bone 86 (2016) 119–130, https://doi.org/10.1016/j.bone.2016.02.020.

[12] J. Lodder, T. Denaës, M.N. Chobert, J. Wan, J. El-Benna, J.M. Pawlotsky, S. Lotersztajn, F. Teixeira-Clerc, Macrophage autophagy protects against liver

fibrosis in mice, Autophagy 11 (2015) 1280–1292, https://doi.org/10.1080/15548627.2015.1058473.
[13] N. Mizushima, B. Levine, A.M. Cuervo, D.J. Klionsky, Autophagy fights disease through cellular self-digestion, Nature 451 (2008) 1069–1075, https://doi.org/10.1038/nature06639.
[14] V. Deretic, T. Saitoh, S. Akira, Autophagy in infection, inflammation and immunity, Nat. Rev. Immunol. 13 (2013) 722–737, https://doi.org/10.1038/nri3532.
[15] Y. Choi, J.W. Bowman, J.U. Jung, Autophagy during viral infection - a double-edged sword, Nat. Rev. Microbiol. 16 (2018) 341–354, https://doi.org/10.1038/s41579-018-0003-6.
[16] A.J. Stranks, A.L. Hansen, I. Panse, M. Mortensen, D.J. Ferguson, D.J. Puleston, K. Shenderov, A.S. Watson, M. Veldhoen, K. Phadwal, V. Cerundolo, A.K. Simon, Autophagy controls acquisition of aging features in macrophages, Journal of innate immunity 7 (2015) 375–391, https://doi.org/10.1159/000370112.
[17] K. Maiese, Warming up to new possibilities with the capsaicin receptor TRPV1: mTOR, AMPK, and erythropoietin, Curr. Neurovascular Res. 14 (2017) 184–189, https://doi.org/10.2174/1567202614666170313105337.
[18] J.M. Bravo-San Pedro, G. Kroemer, L. Galluzzi, Autophagy and mitophagy in cardiovascular disease, Circ. Res. 120 (2017) 1812–1824, https://doi.org/10.1161/circresaha.117.311082.
[19] A. Mantovani, S.K. Biswas, M.R. Galdiero, A. Sica, M. Locati, Macrophage plasticity and polarization in tissue repair and remodelling, J. Pathol. 229 (2013) 176–185, https://doi.org/10.1002/path.4133.
[20] T.A. Wynn, K.M. Vannella, Macrophages in tissue repair, regeneration, and fibrosis, Immunity 44 (2016) 450–462, https://doi.org/10.1016/j.immuni.2016.02.015.
[21] M.Y. Wu, J.H. Lu, Autophagy and macrophage functions: inflammatory response and phagocytosis, Cells 9 (2019) 70, https://doi.org/10.3390/cells9010070.
[22] C.P. Chang, Y.C. Su, C.W. Hu, H.Y. Lei, TLR2-dependent selective autophagy regulates NF-κB lysosomal degradation in hepatoma-derived M2 macrophage differentiation, Cell Death Differ. 20 (2013) 515–523, https://doi.org/10.1038/cdd.2012.146.
[23] V. Byles, A.J. Covarrubias, I. Ben-Sahra, D.W. Lamming, D.M. Sabatini, B. D. Manning, T. Horng, The TSC-mTOR pathway regulates macrophage polarization, Nat. Commun. 4 (2013) 2834, https://doi.org/10.1038/ncomms3834.
[24] L. Zhu, T. Yang, L. Li, L. Sun, Y. Hou, X. Hu, L. Zhang, H. Tian, Q. Zhao, J. Peng, H. Zhang, R. Wang, Z. Yang, L. Zhang, Y. Zhao, TSC1 controls macrophage polarization to prevent inflammatory disease, Nat. Commun. 5 (2014) 4696, https://doi.org/10.1038/ncomms5696.
[25] M.H. Oh, S.L. Collins, I.H. Sun, A.J. Tam, C.H. Patel, M.L. Arwood, Y. Chan-Li, J. D. Powell, M.R. Horton, mTORC2 signaling selectively regulates the generation and function of tissue-resident peritoneal macrophages, Cell Rep. 20 (2017) 2439–2454, https://doi.org/10.1016/j.celrep.2017.08.046.
[26] Y.C. Kim, K.L. Guan, mTOR: a pharmacologic target for autophagy regulation, J. Clin. Invest. 125 (2015) 25–32, https://doi.org/10.1172/jci73939.
[27] H. Zhang, C. Lin, C. Zeng, Z. Wang, H. Wang, J. Lu, X. Liu, Y. Shao, C. Zhao, J. Pan, S. Xu, Y. Zhang, D. Xie, D. Cai, X. Bai, Synovial macrophage M1 polarisation exacerbates experimental osteoarthritis partially through R-spondin-2, Ann. Rheum. Dis. 77 (2018) 1524–1534, https://doi.org/10.1136/annrheumdis-2018-213450.
[28] A. Mercalli, I. Calavita, E. Dugnani, A. Citro, E. Cantarelli, R. Nano, R. Melzi, P. Maffi, A. Secchi, V. Sordi, L. Piemonti, Rapamycin unbalances the polarization of human macrophages to M1, Immunology 140 (2013) 179–190, https://doi.org/10.1111/imm.12126.
[29] S.L. Dahl, A.P. Kypson, J.H. Lawson, J.L. Blum, J.T. Strader, Y. Li, R.J. Manson, W. E. Tente, L. DiBernardo, M.T. Hensley, R. Carter, T.P. Williams, H.L. Prichard, M. S. Dey, K.G. Begelman, L.E. Niklason, Readily available tissue-engineered vascular grafts, Sci. Transl. Med. 3 (2011) 68ra9, https://doi.org/10.1126/scitranslmed.3001426.
[30] N. L'Heureux, N. Dusserre, G. Konig, B. Victor, P. Keire, T.N. Wight, N.A. Chronos, A.E. Kyles, C.R. Gregory, G. Hoyt, R.C. Robbins, T.N. McAllister, Human tissue-engineered blood vessels for adult arterial revascularization, Nat. Med. 12 (2006) 361–365, https://doi.org/10.1038/nm1364.
[31] J.M. Macrae, I. Dojcinovic, O. Djurdjev, B. Jung, S. Shalansky, A. Levin, M. Kiaii, Citrate 4% versus heparin and the reduction of thrombosis study (CHARTS), Clin. J. Am. Soc. Nephrol. : CJASN 3 (2008) 369–374, https://doi.org/10.2215/cjn.01760407.
[32] Y.U. Lee, T. Yi, S. Tara, A.Y. Lee, N. Hibino, T. Shinoka, C.K. Breuer, Implantation of inferior vena cava interposition graft in mouse model, JoVE : JoVE 88 (2014) 51632, https://doi.org/10.3791/51632.
[33] X. Liu, W. Chen, B. Shao, X. Zhang, Y. Wang, S. Zhang, W. Wu, Mussel patterned with 4D biodegrading elastomer durably recruits regenerative macrophages to promote regeneration of craniofacial bone, Biomaterials 276 (2021) 120998, https://doi.org/10.1016/j.biomaterials.2021.120998.
[34] M. Theret, L. Gsaier, B. Schaffer, G. Juban, S. Ben Larbi, M. Weiss-Gayet, L. Bultot, C. Collodet, M. Foretz, D. Desplanches, P. Sanz, Z. Zang, L. Yang, G. Vial, B. Viollet, K. Sakamoto, A. Brunet, B. Chazaud, R. Mounier, AMPKα1-LDH pathway regulates muscle stem cell self-renewal by controlling metabolic homeostasis, EMBO J. 36 (2017) 1946–1962, https://doi.org/10.15252/embj.201695273.
[35] M. Komatsu, S. Waguri, M. Koike, Y.S. Sou, T. Ueno, T. Hara, N. Mizushima, J. Iwata, J. Ezaki, S. Murata, J. Hamazaki, Y. Nishito, S. Iemura, T. Natsume, T. Yanagawa, J. Uwayama, E. Warabi, H. Yoshida, T. Ishii, A. Kobayashi, M. Yamamoto, Z. Yue, Y. Uchiyama, E. Kominami, K. Tanaka, Homeostatic levels of p62 control cytoplasmic inclusion body formation in autophagy-deficient mice, Cell 131 (2007) 1149–1163, https://doi.org/10.1016/j.cell.2007.10.035.
[36] R. Huang, W. Liu, Identifying an essential role of nuclear LC3 for autophagy, Autophagy 11 (2015) 852–853, https://doi.org/10.1080/15548627.2015.1038016.
[37] G. Mariño, M. Niso-Santano, E.H. Baehrecke, G. Kroemer, Self-consumption: the interplay of autophagy and apoptosis, Nat. Rev. Mol. Cell Biol. 15 (2014) 81–94, https://doi.org/10.1038/nrm3735.
[38] J. Fu, M. Wang, I. De Vlaminck, Y. Wang, Thick PCL fibers improving host remodeling of PGS-PCL composite grafts implanted in rat common carotid arteries, Small 16 (2020), e2004133, https://doi.org/10.1002/smll.202004133.
[39] T. Fukunishi, C.S. Ong, P. Yesantharao, C.A. Best, T. Yi, H. Zhang, G. Mattson, J. Boktor, K. Nelson, T. Shinoka, C.K. Breuer, J. Johnson, N. Hibino, Different degradation rates of nanofiber vascular grafts in small and large animal models, Journal of tissue engineering and regenerative medicine 14 (2020) 203–214, https://doi.org/10.1002/term.2977.
[40] Y. Pan, X. Zhou, Y. Wei, Q. Zhang, T. Wang, M. Zhu, W. Li, R. Huang, R. Liu, J. Chen, G. Fan, K. Wang, D. Kong, Q. Zhao, Small-diameter hybrid vascular grafts composed of polycaprolactone and polydioxanone fibers, Sci. Rep. 7 (2017) 3615, https://doi.org/10.1038/s41598-017-03851-1.
[41] K. Liu, E. Zhao, G. Ilyas, G. Lalazar, Y. Lin, M. Haseeb, K.E. Tanaka, M.J. Czaja, Impaired macrophage autophagy increases the immune response in obese mice by promoting proinflammatory macrophage polarization, Autophagy 11 (2015) 271–284, https://doi.org/10.1080/15548627.2015.1009787.
[42] G. Lu, R. Zhang, S. Geng, L. Peng, P. Jayaraman, C. Chen, F. Xu, J. Yang, Q. Li, H. Zheng, K. Shen, J. Wang, X. Liu, W. Wang, Z. Zheng, C.F. Qi, C. Si, J.C. He, K. Liu, S.A. Lira, A.G. Sikora, L. Li, H. Xiong, Myeloid cell-derived inducible nitric oxide synthase suppresses M1 macrophage polarization, Nat. Commun. 6 (2015) 6676, https://doi.org/10.1038/ncomms7676.
[43] Y. Fu, C. Gao, Y. Liang, M. Wang, Y. Huang, W. Ma, T. Li, Y. Jia, F. Yu, W. Zhu, Q. Cui, Y. Li, Q. Xu, X. Wang, W. Kong, Shift of macrophage phenotype due to cartilage oligomeric matrix protein deficiency drives atherosclerotic calcification, Circ. Res. 119 (2016) 261–276, https://doi.org/10.1161/circresaha.115.308021.
[44] V. Deretic, B. Levine, Autophagy balances inflammation in innate immunity, Autophagy 14 (2018) 243–251, https://doi.org/10.1080/15548627.2017.1402992.
[45] Y. Yang, J. Wang, S. Guo, S. Pourteymour, Q. Xu, J. Gong, Z. Huang, Z. Shen, K. Diabakte, Z. Cao, G. Wu, S. Natalia, Z. Tian, H. Jin, Y. Tian, Non-lethal sonodynamic therapy facilitates the M1-to-M2 transition in advanced atherosclerotic plaques via activating the ROS-AMPK-mTORC1-autophagy pathway, Redox biology 32 (2020) 101501, https://doi.org/10.1016/j.redox.2020.101501.
[46] M.G. Yefimova, N. Messaddeq, T. Harnois, A.C. Meunier, J. Clarhaut, A. Noblanc, J. L. Weickert, A. Cantereau, M. Philippe, N. Bourmeyster, O. Benzakour, A chimerical phagocytosis model reveals the recruitment by Sertoli cells of autophagy for the degradation of ingested illegitimate substrates, Autophagy 9 (2013) 653–666, https://doi.org/10.4161/auto.23839.
[47] Y. Ma, L. Galluzzi, L. Zitvogel, G. Kroemer, Autophagy and cellular immune responses, Immunity 39 (2013) 211–227, https://doi.org/10.1016/j.immuni.2013.07.017.
[48] J.P. Lee, A. Foote, H. Fan, C. Peral de Castro, T. Lang, S.A. Jones, N. Gavrilescu, K. H. Mills, M. Leech, E.F. Morand, J. Harris, Loss of autophagy enhances MIF/macrophage migration inhibitory factor release by macrophages, Autophagy 12 (2016) 907–916, https://doi.org/10.1080/15548627.2016.1164358.
[49] R. Singh, A.M. Cuervo, Autophagy in the cellular energetic balance, Cell Metabol. 13 (2011) 495–504, https://doi.org/10.1016/j.cmet.2011.04.004.
[50] Y. Duan, S. Yu, P. Xu, X. Wang, X. Feng, Z. Mao, C. Gao, Co-immobilization of CD133 antibodies, vascular endothelial growth factors, and REDV peptide promotes capture, proliferation, and differentiation of endothelial progenitor cells, Acta Biomater. 96 (2019) 137–148, https://doi.org/10.1016/j.actbio.2019.07.004.
[51] R.J. Smith Jr., B. Nasiri, J. Kann, D. Yergeau, J.E. Bard, D.D. Swartz, S. T. Andreadis, Endothelialization of arterial vascular grafts by circulating monocytes, Nat. Commun. 11 (2020) 1622, https://doi.org/10.1038/s41467-020-15361-2.
[52] S. Morioka, M. Inagaki, Y. Komatsu, Y. Mishina, K. Matsumoto, J. Ninomiya-Tsuji, TAK1 kinase signaling regulates embryonic angiogenesis by modulating endothelial cell survival and migration, Blood 120 (2012) 3846–3857, https://doi.org/10.1182/blood-2012-03-416198.
[53] M. Tariq, J. Zhang, G. Liang, L. Ding, Q. He, B. Yang, Macrophage polarization: anti-cancer strategies to target tumor-associated macrophage in breast cancer, J. Cell. Biochem. 118 (2017) 2484–2501, https://doi.org/10.1002/jcb.25895.
[54] G. Arango Duque, A. Descoteaux, Macrophage cytokines: involvement in immunity and infectious diseases, Front. Immunol. 5 (2014) 491, https://doi.org/10.3389/fimmu.2014.00491.
[55] G. Tossetta, F. Paolinelli, C. Avellini, E. Salvolini, P. Ciarmela, T. Lorenzi, M. Emanuelli, P. Toti, R. Giuliante, R. Gesuita, C. Crescimanno, C. Voltolini, R. Di Primio, F. Petraglia, M. Castellucci, D. Marzioni, IL-1β and TGF-β weaken the placental barrier through destruction of tight junctions: an in vivo and in vitro study, Placenta 35 (2014) 509–516, https://doi.org/10.1016/j.placenta.2014.03.016.
[56] Y. Amir Levy, T.P. Ciaraldi, S.R. Mudaliar, S.A. Phillips, R.R. Henry, Excessive secretion of IL-8 by skeletal muscle in type 2 diabetes impairs tube growth: potential role of PI3K and the Tie2 receptor, Am. J. Physiol. Endocrinol. Metabol. 309 (2015) E22–E34, https://doi.org/10.1152/ajpendo.00513.2014.
[57] S. Naik, S.B. Larsen, C.J. Cowley, E. Fuchs, Two to tango: dialog between immunity and stem cells in health and disease, Cell 175 (2018) 908–920, https://doi.org/10.1016/j.cell.2018.08.071.

[58] I. Sergin, T.D. Evans, X. Zhang, S. Bhattacharya, C.J. Stokes, E. Song, S. Ali, B. Dehestani, K.B. Holloway, P.S. Micevych, A. Javaheri, J.R. Crowley, A. Ballabio, J.D. Schilling, S. Epelman, C.C. Weihl, A. Diwan, D. Fan, M.A. Zayed, B. Razani, Exploiting macrophage autophagy-lysosomal biogenesis as a therapy for atherosclerosis, Nat. Commun. 8 (2017) 15750, https://doi.org/10.1038/ncomms15750.

[59] T.D. Evans, I. Sergin, X. Zhang, B. Razani, Target acquired: selective autophagy in cardiometabolic disease, Sci. Signal. 10 (2017), eaag2298, https://doi.org/10.1126/scisignal.aag2298.

[60] Y. Li, Z. Sun, L. Zhang, J. Yan, C. Shao, L. Jing, L. Li, Z. Wang, Role of macrophages in the progression and regression of vascular calcification, Front. Pharmacol. 11 (2020) 661, https://doi.org/10.3389/fphar.2020.00661.

[61] M. Wu, C. Rementer, C.M. Giachelli, Vascular calcification: an update on mechanisms and challenges in treatment, Calcif. Tissue Int. 93 (2013) 365–373, https://doi.org/10.1007/s00223-013-9712-z.

[62] C.T. Kraft, S. Agarwal, K. Ranganathan, V.W. Wong, S. Loder, J. Li, M.J. Delano, B. Levi, Trauma-induced heterotopic bone formation and the role of the immune system: a review, The journal of trauma and acute care surgery 80 (2016) 156–165, https://doi.org/10.1097/ta.0000000000000883.

[63] X. Zhang, J. Li, J.J. Qin, W.L. Cheng, X. Zhu, F.H. Gong, Z. She, Z. Huang, H. Xia, H. Li, Oncostatin M receptor β deficiency attenuates atherogenesis by inhibiting JAK2/STAT3 signaling in macrophages, J. Lipid Res. 58 (2017) 895–906, https://doi.org/10.1194/jlr.M074112.

[64] R. Villa-Bellosta, M.R. Hamczyk, V. Andrés, Alternatively activated macrophages exhibit an anticalcifying activity dependent on extracellular ATP/pyrophosphate metabolism, Am. J. Physiol. Cell Physiol. 310 (2016) C788–C799, https://doi.org/10.1152/ajpcell.00370.2015.

[65] T.T. Braga, J.S. Agudelo, N.O. Camara, Macrophages during the fibrotic process: M2 as friend and foe, Front. Immunol. 6 (2015) 602, https://doi.org/10.3389/fimmu.2015.00602.

[66] J.L. Kaplan, M.A. Marshall, C.M. C, D.B. Harmon, J.C. Garmey, S.N. Oldham, P. Hallowell, C.A. McNamara, Adipocyte progenitor cells initiate monocyte chemoattractant protein-1-mediated macrophage accumulation in visceral adipose tissue, Molecular metabolism 4 (2015) 779–794, https://doi.org/10.1016/j.molmet.2015.07.010.

[67] A. Lindhorst, N. Raulien, P. Wieghofer, J. Eilers, F.M.V. Rossi, I. Bechmann, M. Gericke, Adipocyte death triggers a pro-inflammatory response and induces metabolic activation of resident macrophages, Cell Death Dis. 12 (2021) 579, https://doi.org/10.1038/s41419-021-03872-9.

[68] G. Luo, Q. Yang, B. Yao, Y. Tian, R. Hou, A. Shao, M. Li, Z. Feng, W. Wang, Slp-coated liposomes for drug delivery and biomedical applications: potential and challenges, Int. J. Nanomed. 14 (2019) 1359–1383, https://doi.org/10.2147/ijn.S189935.